

# Urban heat island and pollutant correlations in Bangalore, India using geospatial techniques

Aneesh Mathew <sup>\*</sup>, K.S. Arunab 

Department of Civil Engineering, National Institute of Technology, Tiruchirappalli, 620015, Tamil Nadu, India

## ARTICLE INFO

**Keywords:**  
 Urban heat island effect  
 Thermal classification  
 Air pollution  
 High-risk zones

## ABSTRACT

The interaction between urban heat island (UHI) effects and urban air pollution significantly impacts urban ecology, climate dynamics, and inhabitants' well-being. This study examines into the correlation between UHI effects and various pollutants (CO, HCHO, aerosols, NO<sub>2</sub>, O<sub>3</sub>, and SO<sub>2</sub>) across Bangalore from 2019 to 2022, exploring their spatial and thermal connections. The study utilized satellite remote sensing data from TROPOMI for air pollutants (CO, NO<sub>2</sub>, HCHO, SO<sub>2</sub>, O<sub>3</sub>, and aerosols) and MODIS for land surface temperature (LST). Data were collected over a four-year period (2019–2022) to analyze spatial and temporal pollutant distributions and UHI effects in Bangalore and employed statistical methods, including Pearson correlation, independent *t*-tests, and ANOVA, to assess the relationships between UHI indicators and pollutant concentrations. A weighted Urban Pollution Island (UPI) index was developed using Fuzzy AHP, while thermal categorization was achieved through spatial analysis techniques. Research indicates significantly elevated pollution levels in urban areas compared to rural regions. The research demonstrates positive correlation between UHI indicators and CO, HCHO, aerosols, NO<sub>2</sub>, and O<sub>3</sub> in urban-rural environments. A negative correlation is observed between the UHI indicator and SO<sub>2</sub> in these contexts, requiring a thorough investigation of the UHI-pollutant relationship. High-risk zones (HRZs) demonstrate significantly elevated yearly average concentrations of NO<sub>2</sub> (66.614%), aerosols (13.610%), HCHO (8.816%), and CO (2.028%) relative to low-risk zones (LRZs). Ozone levels are consistently similar between HRZs and LRZs. In contrast, LRZs demonstrate a greater yearly average concentration of SO<sub>2</sub> (7.562%) than HRZs. Furthermore, HRZs exhibit an elevated LST of 2.198 °C relative to LRZs. These results yield essential insights for urban planning and policy development, providing a thorough comprehension of UHI pollution dynamics. This research clarifies these dynamics, aiding informed decision-making to mitigate the effects of UHI and pollution in urban settings.

## 1. Introduction

Rapid urban growth has resulted in widespread infrastructure development, replacing natural ecosystems with heat-absorbing surfaces like roads and buildings. This transformation contributes to the UHI effect, a phenomenon where urban or metropolitan areas experience significantly higher temperatures than surrounding rural areas due to human activities and changes in land cover [1,2]. Urban areas experience higher temperatures, especially at night. Unplanned urban expansion exacerbates these environmental challenges by increasing heat stress and air pollution. The reduction of green spaces further intensifies the UHI effect, as vegetation plays a crucial role in cooling urban areas [3,4]. UN EPA [5] projected that the global urban population, which stood at approximately 750 million in 1951, will rise to

approximately 9.7 billion by 2050. This unregulated population growth results in unplanned, rapid, and unsustainable urban expansion. Thus, local and global ecosystems have suffered. Due to concerns about urban air quality and the urban heat island effect, urban ecology's public health aspect has grown [5]. UHI develop when natural and human factors boost urban temperatures above rural levels [6–8]. In calm weather, nighttime temperature contrast is greater than daytime. UHI is strongest in winter and summer. Surface heat absorption and retention determine rural-urban temperature [9].

UHI-induced heat stress can cause heat stroke, heat exhaustion, cramps, or rashes, and it has also been associated with an increase in suicidal thoughts [10,11]. UHI can change and disturb the air distribution pattern around urban areas, resulting in rainfall in neighbouring areas and new ecological consequences [12]. UPI and UHI are results of

\* Corresponding author.

E-mail addresses: [aneesh@nitt.edu](mailto:aneesh@nitt.edu), [aneesh52006@gmail.com](mailto:aneesh52006@gmail.com) (A. Mathew).

substantial alterations in residential zones, energy utilization patterns, transportation methods, and commercial practices. Rapid urbanization, population expansion, and continuous migration into metropolitan areas exert pressure on natural resources, resulting in these alterations [13]. Combustion processes in industry, transportation, and human activities such as air conditioning and cooking are intimately associated with UPI and UHI as producers of heat and pollution. UHI impacts community quality of life and ecology, considering local and global urban ecosystem disruptions and climate change [14,15].

In urban areas, impermeable surfaces such as roads, plazas, parking lots, and structures supplant natural permeability and vegetation [16, 17]. Cities and towns with impermeable surfaces are much hotter than rural areas in the summer. Heat-absorbing cities are especially vulnerable to excessive heat. This influence may harm metropolitan life and public health [18]. The UHI impact is fluctuations in aerosol load, land cover, and surface UHI formation over Delhi [19], and their data showed that Delhi afternoon temperatures are almost always higher than nearby places. The minimum night heat occurs in the range of 0–2 K, while the maximum is between 4 and 6 K during the monsoon and March. UHI effects during day and night are contingent upon land cover features, including developed areas, bare soil, and vegetation, as indicated by statistical data. In July 2009, Kourtidis et al. [20] employed air temperature and humidity data to delineate the hourly urban heat island effect across 26 sites in Athens, Greece. The research indicated that urban areas next to the eastern highlands experienced the highest afternoon temperatures and the lowest morning temperatures. Mean wind flow was demonstrated to influence temperatures, although it did not affect the daily progression of UHI.

Mathew et al. [21] analyzed the spatial and seasonal fluctuations of UHI effects over Jaipur, highlighting their strong correlations with vegetation cover, urban development, and elevation parameters. Their findings emphasized that built-up areas and sparse vegetation significantly contribute to higher UHI intensity. Grigoraş and Urişescu [22] investigated the relationship between air temperature and LST in Bucharest, Romania's capital, and identified hot zones. The analysis included data from four automated weather stations and Terra and Aqua MODIS imagery throughout the summer of 2017. The correlation between LST and air temperature was strongest at night (0.8–0.87) and weaker during the day (0.7–0.77). The Getis-Ord spatial statistics analysis indicated hot zones, and satellite data was compared with in-situ temperature measurements. In densely populated residential neighborhoods and city center thoroughfares, "very hot" locations were the most prevalent. These "very hot spots" encompassed 33.2% of the city during the day and 31.6% at night. Throughout the day and night, 27.1% of the city center was "very hot."

Shahfahad et al. [23] showed that most cities feature impermeable surfaces like concrete, glass, and metal, which absorb and reflect heat, increasing LST. Urban hotspots are excessive LST surfaces with high temperatures. UHI must be identified and monitored to mitigate temperature and sustain urban ecosystem. UHI research relies on the Urban Thermal Field Variation Index (UTFVI) to measure urban thermal ecology positions based on LST and create thermal maps. UTFVI hotspots are often found in rural, highly populated, and concrete-heavy areas, which might affect surface UHI impacts.

The interaction between air pollution and LST may be complex. Air pollutant concentration and presence might be LST, affecting their dispersal and behavior. High levels of particulate matter, ozone, and CO<sub>2</sub> may trap heat in the lower atmosphere [1,24]. The UHI effect can be exacerbated by elevated LST in metropolitan regions with high pollutant levels [25,26]. Aerosols affect cloud formation and properties [22]. This interaction may affect LST [5,27]. Temperature and air quality depend on vegetation. Trees and vegetation absorb pollutants and release oxygen, reducing air pollution. They also shade and evapotranspiration, lowering urban LST and UHI [28,29]. Regional weather conditions, terrain, urban morphology, and pollutant characteristics can impact the relationship between air pollutants and LST [28]. Thus, investigating

LST and air pollutants involves a full investigation of these parameters and their interactions [30]. On the connection between UHI and UPI, Ulpiani [31] conducted a detailed review of the gathered information on the relationship between UHI and UPI since 1990. To identify methodological and experimental trends, geographical interdependence, and research gaps, the outcomes of 16 nations and 11 Köppen-Geiger climate regions are examined and differentiated.

Human circumstances have improved with urbanization. The convenience and superior quality of urban living have profoundly influenced environmental issues arising from urbanization, including global warming, air pollution, and ecological degradation. By 2030, metropolitan cities are projected to house more than five billion individuals [22]. Land will endure substantial detriment as large populations migrate to urban areas. Urban expansion constitutes a significant environmental challenge [32,33]. Consequently, UHI studies are crucial for informing urban planning and development in developing countries such as India. The UHI impact may be intensified by increased land surface temperatures in urban regions with increasing pollution concentrations [26,34]. Policymakers and urban planners can manage fast urbanization and ensure sustainable urban expansion by researching UHI effects [35,36].

Air pollution substantially influences the urban heat island effect, underscoring the need of investigating their interaction [22]. The seasonal and regional distribution of urban heat islands in relation to air pollution features can aid in mitigating their effects in the future. This study finds sites with elevated UHI intensity, enabling researchers to explore cause-and-effect relationships and recommend locations for targeted mitigation [37]. Researchers investigate air pollution and urban heat islands to enhance urban planning and development. This research delineates UHI mitigation strategies and inform decision-making to cultivate more sustainable and resilient urban environments [31].

Previous studies have focused either on the UHI effect or on air pollution, but very few have explored the intricate relationship between these two phenomena in a holistic manner [38]. There is limited research that integrates spatial and seasonal variations of UHI intensity with air pollution parameters. Furthermore, the role of specific pollutants in amplifying the UHI effect, particularly in the context of urban planning, has not been thoroughly examined. This research offers a novel approach by combining satellite remote sensing data and ground-level air quality measurements to study the seasonal and spatial distribution of UHI with respect to air pollution. It seeks to identify UHI hotspots, which will help in devising localized strategies for urban planning and environmental management. The primary aim of this research is to comprehensively analyze the relationship between UHI and air pollutants using satellite remote sensing and ground-level air quality data and to identify hotspots of UHI intensity for targeted mitigation strategies. The objectives of this study encompass i) To quantify the UHI intensity using satellite remote sensing data. ii) To identify and analyze hotspots of UHI intensity and air pollution by integrating LST and air quality data. iii) To establish correlations between different pollutants and UHI intensity to understand their interactions and effects on urban environments. These objectives collectively form a comprehensive approach to better understanding the complex relationship between air quality and urban heat islands, providing useful insights into urban planning, environmental management, and public health policies.

## 2. Study area and its features

Bangalore, situated in the southern part of India on the Mysore Plateau, boasts a mean elevation of 900 m and is part of the larger Cretaceous Deccan Plateau. The area encompasses 741 km<sup>2</sup> and is situated at 12°58'44"N 77°35'30"E. Recent projections and demographic trends estimate Bangalore's population to be approximately 14,008,300 as of 2024 [39]. Bangalore ranks as the 18<sup>th</sup> most populated city in the world and is the sixth most populous urban agglomeration in India.

Between 1991 and 2001, Bangalore recorded the highest growth rate in India, attaining a 38% increase during the decade [40]. Bangalore, the capital of Karnataka, India, is primarily level, save for the hilly western areas. Vidyaranyapura Doddabettahalli, situated in the northwest, is the city's highest peak, rising to an elevation of 962 m (3156 ft) above sea level. [Fig. 1](#) depicts the geographical location of the Bangalore research area.

Bangalore experiences distinct wet and dry seasons and is categorized as a tropical savanna according to the Köppen climate classification (Aw). The city's elevated altitude results in generally moderate temperatures throughout the year, however intermittent heat waves may render summers miserable. Rainfall is delivered by both the northeast and southwest monsoons, influencing the city's seasonal fluctuation [40].

### 3. Data and methodology

This research aims to analyze both the geographical and seasonal distribution of pollutants over a 4-year period spanning from 2019 to 2022. Data regarding pollutants is sourced from the TROPOspheric Monitoring Instrument (TROPOMI), a satellite instrument on board Sentinel-5, and MODIS. By examining variations in levels of pollutants within both urban and rural settings, the goal is to detect any irregularities. In tropical regions with extensive bare soil, night time LST is particularly adept at capturing UHI effects compared to daytime LST. This is because night time LST is more sensitive to thermal changes during the nighttime, offering a thorough understanding of UHI dynamics in such ecosystems [33]. The MODIS sensor acquires nighttime LST, which serves as the foundation for evaluating the impact of UHI events [41,42]. A measure of a particular condition of UHI, named  $UHI_{index}$ , is employed to classify the research area into zones undergoing either high or low thermal stress [43]. The associations between

contaminants and the UHI indicator are developed using Pearson correlation analysis [44]. Furthermore, an all-encompassing measure named  $UHI_{index}$  is developed [45,46]; this approach considers the impact of each contaminant at precise spatial and seasonal coordinates throughout the complete research region. Tukey's HSD was applied after conducting the ANOVA to explore further pairwise comparisons between the zones, ensuring that significant differences were identified at a confidence level of 95%. Additionally, a pollutant risk map is created based on clustering the levels of contaminants in a spatial manner. Classifying areas within the research region as severely, moderately, or least contaminated. The methodology illustrating the sequence of steps or processes in a visual format is depicted in [Fig. 2](#).

#### 3.1. Data used

This study employs satellite-derived pollutants, such as  $O_3$ , aerosols,  $SO_2$ ,  $HCHO$ ,  $NO_2$ ,  $CO$ , and LST, to examine the relationship between UHI effects and air contaminants. [Table 1](#) delineates the dataset employed and its parameters.

The study utilized daily data from sources including TROPOMI and MODIS to gather information on pollution annually and seasonally. This research employed daily Aerosol Optical Depth photos from the MODIS component MCD19A2. The MOD11A2 package supplied the requisite nighttime land surface temperature data for this investigation.

#### 3.2. Land cover categorization and distinguishing of urban-rural regions

During the summer seasons of the research period, we captured numerous spectral bands without cloud cover and used them to categorize the land cover of the Bangalore area in images from the Landsat 8 satellite. Google Earth Engine's SMILE Random Forest machine learning algorithm performed the classification [47,48]. By analyzing images

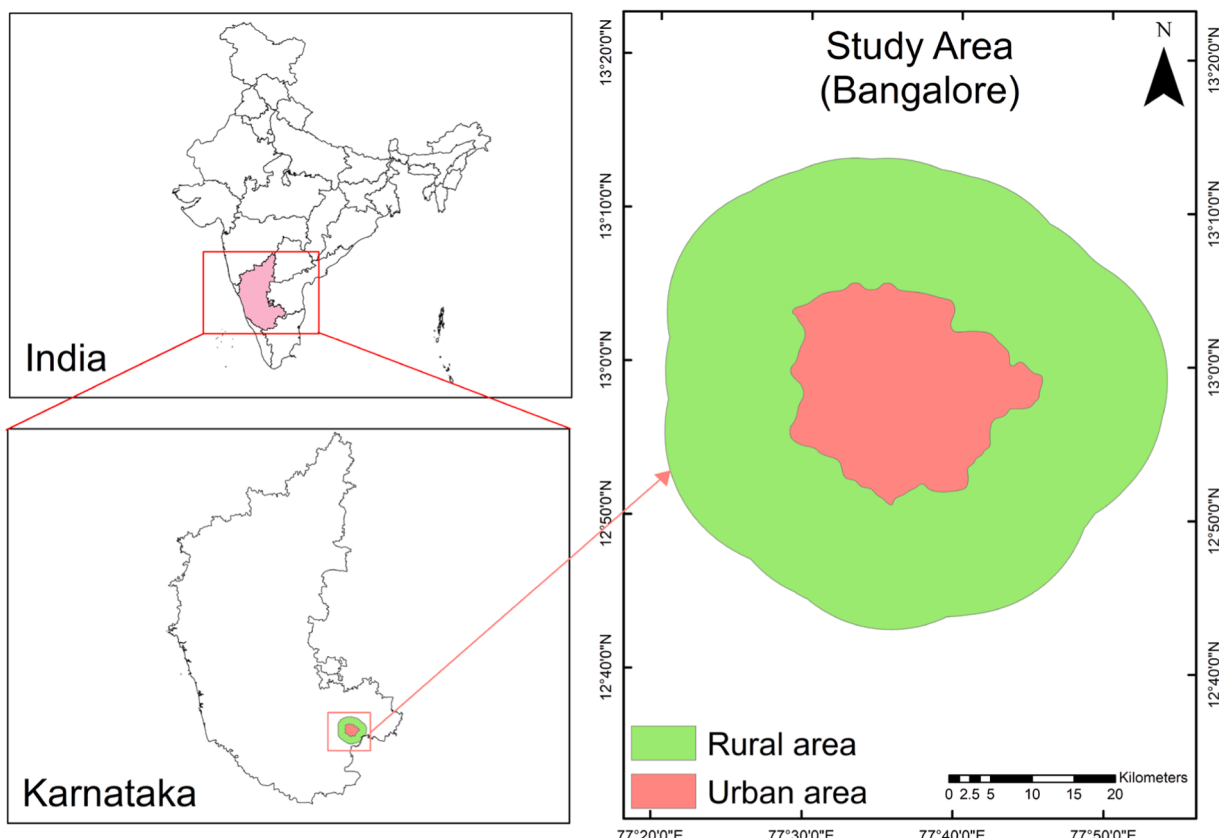


**Fig. 1.** The geographical location of Bangalore, highlighting its urban boundaries and surrounding rural areas.

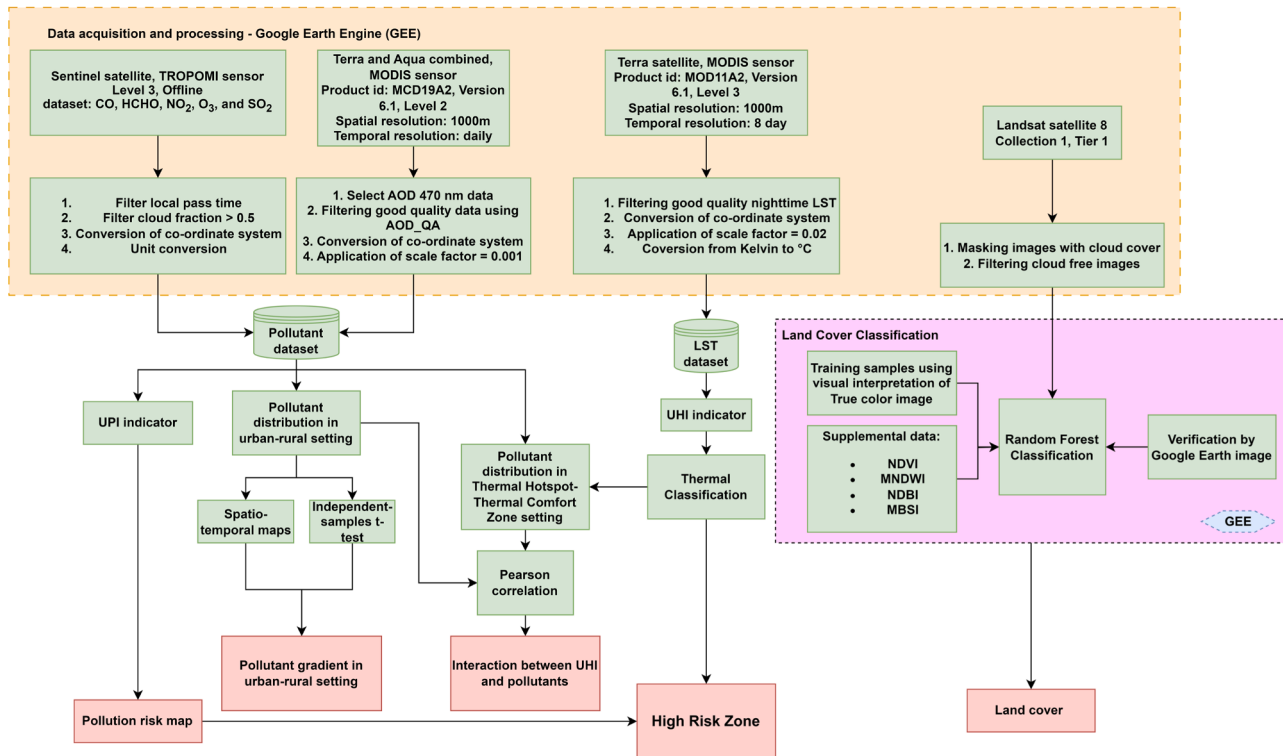


Fig. 2. Flowchart of methodology.

**Table 1**  
LST and pollutant dataset used in the research.

Dataset	Sensor	Band/Product
O <sub>3</sub> , LST	MODIS	MOD11A2/ LST_Night_1km O3_column_number_density
AOD (Aerosols)		MCD19A2/Optical_Depth_047
SO <sub>2</sub>	TROPOMI	SO2_column_number_density
HCHO		tropospheric_HCHO_column_number_density
NO <sub>2</sub>		tropospheric_NO2_column_number_density
CO		CO_column_number_density
O <sub>3</sub>		O3_column_number_density

using their texture and incorporating additional spectral indices like the Modified Normalized Difference Water Index (MNDWI), the Normalized Difference Vegetation Index (NDVI), the Modified Bare Soil Index (MBSI), and the Normalized Difference Built-up Index (NDBI), we further improved the classification [49–52]. Supplemental spectral indices improved the classifier's reliability by giving valuable data points for training and validation. According to Kavhu et al. [53] & Setturu et al. [54], the variety of these spectral indices, which included NDBI, MBSI, NDVI, and MNDWI, significantly contributed to the robustness of the LULC classifier. This enhanced classifier was able to divide the research area into four major land cover types: construction zones, bare soil regions, water bodies, and vegetation areas.

The spectral indices MNDWI, NDVI, MBSI, and NDBI [50–52] are computed utilizing Eqs. (1), 2, 3, and 4, respectively.

$$MNDWI = \frac{GREEN - SWIR1}{GREEN + SWIR1} \quad (1)$$

$$NDVI = \frac{NIR - RED}{NIR + RED} \quad (2)$$

$$MBSI = \frac{SWIR1 - SWIR2 - NIR}{SWIR1 + SWIR2 + NIR} + 0.5 \quad (3)$$

$$NDBI = \frac{SWIR1 - NIR}{SWIR1 + NIR} \quad (4)$$

Where

NIR = Near-infrared band

RED = Red band

GREEN = Green band

SWIR1 = Shortwave infrared 1

SWIR2 = Shortwave infrared 2

Bangalore's urban limit is defined by the LULC categorization, which uses built-up regions to identify urban and semi-urban areas. The research imposes a 15 km buffer from this urban border to accommodate a sizable rural region.

### 3.3. Statistical analysis

The research used the independent samples t-test to ascertain whether there are main differences in contaminant levels between urban and non-urban locations [55]. The investigation of the influence of fluctuation on air in UHI contaminants by Pearson correlation [56].

### 3.4. UHI indicator

This investigation focuses on exploring the effects of UHI during night-time, driven by the extensive areas of desolate terrain within the study area. The reasoning is based on the observation that regions with limited or large tracts of barren land and moderate vegetation show different patterns in daytime and nighttime LST imagery. Daytime patterns can vary widely due to complex interactions with solar radiation, leading to significant temporal fluctuations [33]. Conversely, nocturnal patterns exhibit more stability, making night-time LST imaging more appropriate for evaluating and quantifying UHI impacts using the UHI<sub>index</sub> [57]. The UHI<sub>index</sub> can be computed using Eq. (5) [58,59].

$$UHI_{index} = \frac{LST_i - LST_{min}}{LST_{max} - LST_{min}} \quad (5)$$

Where,

$LST_i$  = LST of the  $i^{\text{th}}$  spatial point,  
 $LST_{\min}$  = minimum LST of the spatial expanse, and  
 $LST_{\max}$  = maximum LST of the spatial expanse.

### 3.5. UPI indicator

Although spatial and seasonal maps often highlight specific contaminants, it is important to assess the combined effects of various contaminants in the atmosphere [60]. This broader perspective is key to understanding the cumulative effects of pollutants across different regions and their relationship with UHI effects. Recognizing the limitations of conventional approaches, this study presents a framework to measure the Urban Pollution Island index ( $UPI_{\text{index}}$ ). The  $UPI_{\text{index}}$  represents the aggregate pollution levels at specific locations and times. It is derived using Eqs. (6) and 7, offering a structured method for calculating this integrated metric.

$$X_{\text{index}} = \frac{X_i - X_{\min}}{X_{\max} - X_{\min}} \quad (6)$$

Where,

$X_i$  = pollutant value at a pixel (a particular spatial point),  
 $X_{\max}$  = maximum pollutant value in the study region,  
 $X_{\min}$  = minimum pollutant value in the study region.

$$UPI_{\text{index}} = W_{CO} \times CO_{\text{index}} + W_{HCHO} \times HCHO_{\text{index}} + W_{AOD} \times AOD_{\text{index}} + W_{NO_2} \times NO_2_{\text{index}} + W_{O_3} \times O_3_{\text{index}} + W_{SO_2} \times SO_2_{\text{index}} \quad (7)$$

Where,

$W_{CO}$ ,  $W_{HCHO}$ ,  $W_{AOD}$ ,  $W_{NO_2}$ ,  $W_{O_3}$ ,  $W_{SO_2}$  are the weights resulted for each pollutant using the Fuzzy logic and AHP.

A flowchart describing the methodological framework used to assess the UPI indicator is shown in Fig. 3.

To determine how much pollution varies between urban and non-urban locations, the independent sample  $t$ -test is used. The AHP takes these variations as inputs. As a result, giving weights to particular pollutants by using the AHP technique allows for a full assessment of their relevance. To maintain consistency and error-free pairwise comparison matrices in the AHP [61,62], rigorous methods necessitate a detailed evaluation of the relative relevance of different contaminants. Instead of using exact (crisp) values, the research proposes fuzzy triangular numbers to account for any mistakes in the pairwise comparison matrix. This technique improves the robustness of the analysis, enabling more effective handling of imprecise or uncertain data [63].

Using Buckley's fuzzy geometric mean approach (1985), the fuzzy geometric mean for every criterion and fuzzy weights are calculated. Defuzzification is the process of transforming these fuzzy results into more comprehensible and analyzed values [64]. De-fuzzification is a crucial step in the Fuzzy-AHP process, as it converts the triangular fuzzy numbers (TFNs), which represent a range of possible values, into a single crisp value. This step is necessary to derive precise, actionable weights from the fuzzy inputs. The use of fuzzy numbers helps account for uncertainty and variability in expert judgements, but the final decision-making requires definitive weights. De-fuzzification averages the lower, middle, and upper bounds of the fuzzy numbers to generate a single representative value. This ensures the accounting of uncertainty and yields a set of weights directly applicable to the decision-making process. Without this step, the results would remain imprecise, making it difficult to utilize the computed weights effectively. This method uses average and normalized weights to turn fuzzy findings into accurate numerical values. The  $UPI_{\text{index}}$  is computed using the normalized weights generated by the Fuzzy-AHP method for each pollutant. This paradigm addresses uncertainty in the estimation of cumulative levels of pollutants across time and geography by using a methodical, data-driven approach. Being a dimensionless metric, the  $UPI_{\text{index}}$  may represent any combination of contaminants. This measure's versatility allows its

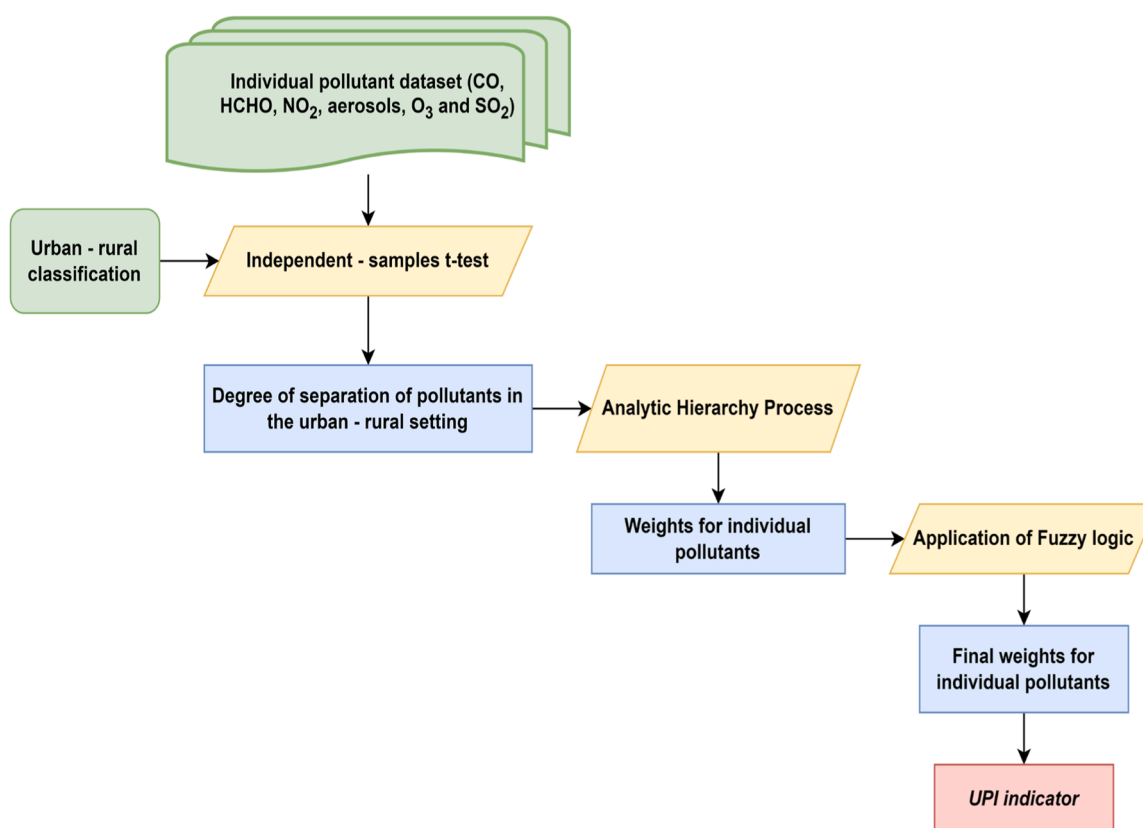


Fig. 3. Methodological framework for calculating UPI indicator.

application in various temporal and geographical contexts.

### 3.6. Thermal categorization of the research region and pollution risk map

The UHI and UPI indicators' geographic distribution can be classified as random, clustered, or dispersed based on the Global Moran's I statistic [65]. In addition, the Getis-Ord  $G^*$  statistic is computed for each pixel in the UHI/UPI indicators to provide thermal categorization and pollution risk maps [66,67]. These maps demonstrate geographic clustering patterns, with z-scores indicating regions with substantial cold spots (low values) and hot spots (high values).

Areas where high  $UHI_{index}$  values cluster (reflecting significant UHI effects) are classified as Thermal Hot Spots (THS), while regions with a concentration of moderate or low  $UHI_{index}$  values (indicating moderate or low UHI effects) are designated as Thermal Cold Zones. Similarly, areas with peak  $UPI_{index}$  values, showing a peak concentration of pollutants, are labeled as High Contamination Zones (HCZ), while regions with moderate and low  $UPI_{index}$  values are classified as Moderate Contamination Zones (MCZ) and Low Contamination Zones (LCZ), respectively.

The methodology evaluates each pixel in relation to the adjacent pixels. Only when surrounded by other high-value pixels does a high-value pixel become a statistically significant hot spot. This assessment entails comparing the local pixel value summation and its neighbours to the overall pixel value summation. When the local sum markedly deviates from the anticipated value, above what random chance would provide, a statistically significant z-score is produced. When the local sum markedly diverges from the anticipated value, and this divergence surpasses what may be attributed to random chance, a statistically significant z-score is generated. The z-score/ $G_i^*$  value is determined using Eq. (8). The  $S$  and  $\bar{X}$  values necessary for calculating the z-score are estimated using the Eq. (9) and 10, respectively [68].

$$G_i^* = \frac{\sum_{j=1}^n w_{ij}x_j - \bar{X}\sum_{j=1}^n w_{ij}}{S\sqrt{\left[\frac{n\sum_{j=1}^n w_{ij}^2 - \left(\sum_{j=1}^n w_{ij}\right)^2}{n-1}\right]}} \quad (8)$$

$$S = \sqrt{\frac{\sum_{j=1}^n x_j^2}{n} - (\bar{X})^2} \quad (9)$$

$$\bar{X} = \frac{\sum_{j=1}^n x_j}{n} \quad (10)$$

Where,

$n$  = the total number of features,  $w_{ij}$  = the spatial weight between feature  $i$  and  $j$ , and  $x_j$  = the attribute value for feature  $j$ .

Ultimately, the overlap between the thermal categorization map and the contaminant risk map helps identify areas that are significantly affected by both intense heat and poor air quality.

### 3.7. Analysis of variance (ANOVA)

Suthar et al. [69] proficiently utilized ANOVA to investigate the correlation between air pollutants and land surface temperature LST. Their analysis focused on evaluating average variations across several groups and assessing the impact of each specific air pollution on LST fluctuations. The study used ANOVA to investigate potential differences in pollutant dispersion and LST across various pollution zones determined by the UPI indicator.

The ANOVA utilises many statistical measures, such as the F-value, which determines if group mean variability exceeds group variability. With a higher F-value, group means are more likely to deviate; the mean square is the average of the squared deviations and is calculated by dividing the sum of squares by the degrees of freedom. It provides a measure of variance within the data; the sum of squares quantifies the

total variability in the data. It is divided into two components: the between-group sum of squares (SSB), which measures the variability between group means, and the within-group sum of squares (SSW), which measures variability within each group, and significance levels assess the probability that the observed differences occurred by chance. Typically, a p-value less than 0.05 is considered statistically significant, indicating that the differences between groups are meaningful and not due to random variation, to comprehensively evaluate the variability in pollutant levels across different zones. In order to provide a more precise measurement of these variations, the analysis incorporates a Post-Hoc investigation, which provides a deeper understanding of the average disparities in pollutant levels among different areas. It also gives further information about standard errors and the relevance of these differences.

## 4. Results and discussion

### 4.1. Spatial and temporal distribution of pollutants

Spatial and seasonal variation of the mean yearly contaminant concentration levels in Bangalore is shown in Fig. 4. The HCHO and CO concentrations exhibited a noteworthy west-to-east gradient, with higher levels observed in the western portion and lower concentrations in the eastern portion of the research region. Urban areas report elevated CO and HCHO levels, indicating that human activities have a major effect on air quality. The prevalence of high aerosol and  $NO_2$  concentrations in the majority of urban areas further underscores the impact of urbanization on pollutant dispersion. Conversely, rural areas generally exhibited lower concentrations of aerosols and  $NO_2$ , with only isolated areas exhibiting heightened pollutant levels. The spatial-temporal maps did not reveal a discernible spatial or temporal pattern in the distribution of  $O_3$  and  $SO_2$  concentrations. While  $SO_2$  does not exhibit a clear, consistent spatial or temporal pattern like  $NO_2$  or aerosols, certain rural areas show elevated  $SO_2$  levels due to localized sources such as industrial activities or agricultural practices.

The independent sample  $t$ -test gave results that compared pollution levels in urban and non-urban locations, as shown in Table 2. The  $t$ -values for total contaminants, with the exception of  $SO_2$ , are statistically significant, indicating that metropolitan areas have greater pollutant concentrations. The largest differences in  $t$ -values were observed for  $NO_2$ , followed by aerosols,  $O_3$ , CO, and HCHO. As shown in Table 2, the p-values for these pollutants, except for  $SO_2$ , were statistically significant ( $p < 0.05$ ), indicating that the differences in pollutant concentrations across regions are meaningful. The urban-rural gradient in the yearly average  $SO_2$  levels in Bangalore and the average  $SO_2$  levels in Bangalore during the summer season is found to be minor. The  $SO_2$  levels in Bangalore's rural regions are greater than in metropolitan areas.

The spatiotemporal maps for  $NO_2$ , HCHO, CO, and aerosols clearly illustrate that pollution levels are constantly higher in cities than in rural areas. In contrast, the spatial-temporal maps for  $O_3$  and  $SO_2$  showed no apparent difference in contaminant levels across urban and non-urban locations. However, an independent samples  $t$ -test of the 4-year annual mean pollutant levels indicated that concentrations of aerosols,  $O_3$ ,  $NO_2$ , CO, and HCHO were significantly higher in urban areas compared to rural areas.  $SO_2$  concentrations are significantly elevated in the urban areas of Bangalore compared to its rural counterparts. In Bangalore, the concentration of  $SO_2$  has an inverse trend, with urban areas showing lower levels than rural regions.

### 4.2. UHI indicator

The spatial pattern of the UHI index reveals that while the urban regions exhibit the highest UHI values [21], certain areas in the southwestern part of the rural section also show relatively higher UHI index values. A combination of factors, including sparse vegetation cover, isolated industrial activities, and heat-absorbing surfaces in this region,

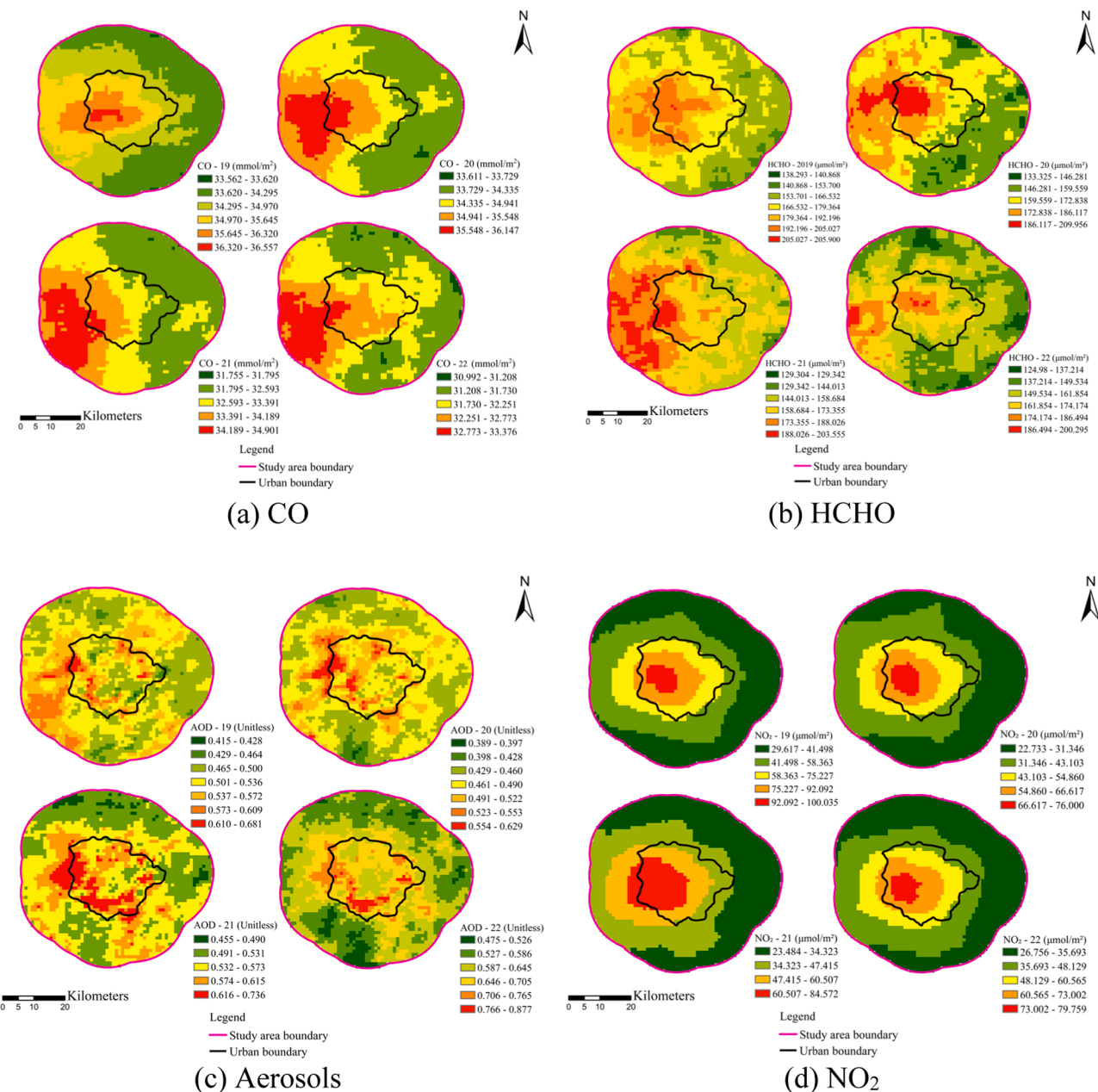


**Fig. 4.** Spatial and seasonal variations in the mean yearly concentrations of key pollutants ((a) CO, (b) HCHO, (c) aerosols, (d) NO<sub>2</sub>, (e) O<sub>3</sub>, (f) SO<sub>2</sub>) in Bangalore from 2019 to 2022.

contribute to this localized increase. These conditions result in localized heat retention, leading to somewhat elevated UHI values compared to other rural areas. However, these levels remain lower than those observed in the core urban zones. **Fig. 5** visually captures the spatial variation of these patterns, highlighting the distribution of UHI across both urban and rural areas.

#### 4.3. Thermal categorization of the research region

**Fig. 6** shows the thermal categorization of the region of study, distinguishing it into Thermal Hot Spots (THSs), Thermal Comfort Zones (TCZs), and Thermal Cold Spots (TCSs). The z-score indicates a statistical chance of less than 1% that the observed clustering pattern is a result of random probability. The thermal categorization map identifies the regions that consistently experienced significantly higher

temperatures compared to the other research areas during the study period (2019–2022).

Temperatures in the THS zones are higher than the mean value for the region when compared to the TCZ, as seen in **Fig. 7**. In THS regions, average temperature is 2.1°C higher than in TCZ areas. Elevated temperatures in THS areas might lead to a variety of negative health repercussions for the people.

#### 4.4. Interaction of night-Time UHI and air pollutants

**Table 3** illustrates the correlation between different air pollutants and the UHI<sub>index</sub>. In metropolitan areas, there is a modest but considerable positive relationship between the particular contaminant and UHI<sub>index</sub> including NO<sub>2</sub>, HCHO, and CO. This indicates that higher UHI effects are associated with increased levels of these pollutants, implying

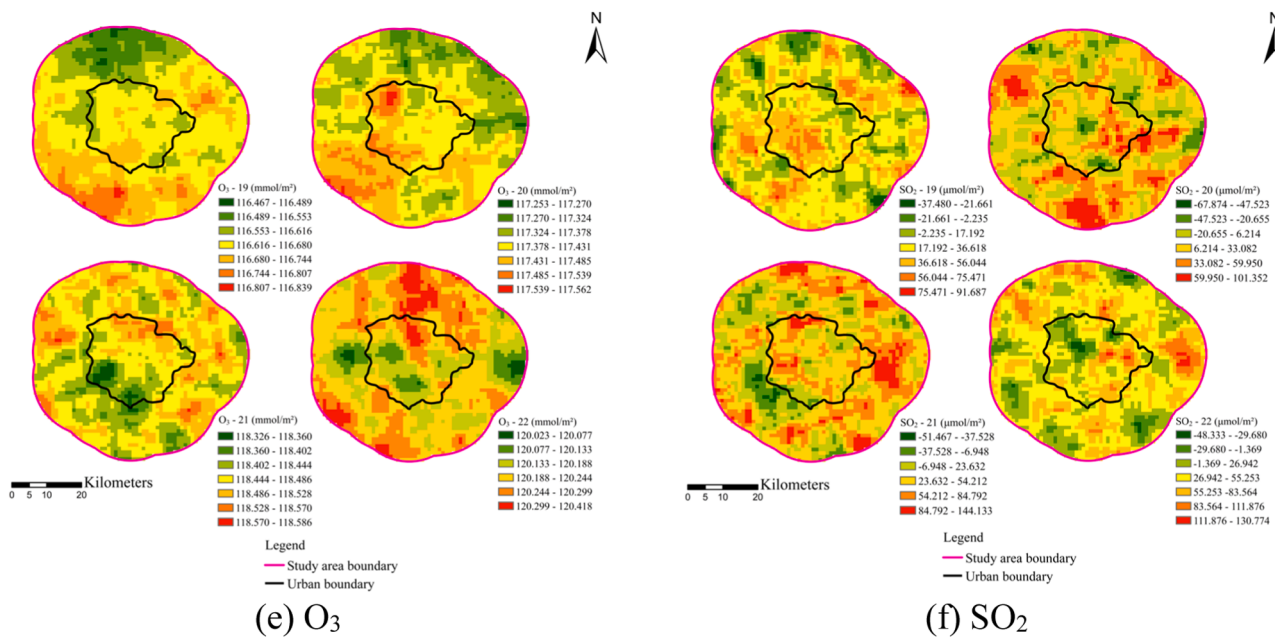


Fig. 4. (continued).

Table 2

Independent samples *t*-test for 4-year annual pollution levels in urban and non-urban locations.

Region/Season	Pollutant	t	df	Sig.	Mean Difference	Std. Error Difference
Bangalore/Annual	CO	16.976	2715	<.001	.476	.028
	HCHO	20.694	2715	<.001	10.555	.510
	AOD	27.367	2715	<.001	.043	.002
	$NO_2$	58.157	2715	.000	24.989	.430
	$O_3$	1.747	2715	.040	-.002	.001
	$SO_2$	-.136	2715	.446	-.074	.547
Bangalore/Summer	CO	27.844	2715	<.001	.675	.024
	HCHO	22.991	2715	<.001	10.861	.472
	AOD	27.291	2715	<.001	.058	.002
	$NO_2$	65.488	2715	.000	21.358	.326
	$O_3$	10.797	2715	<.001	.028	.003
	$SO_2$	-6.386	2715	<.001	-4.921	.771
Bangalore/Winter	CO	11.017	2715	<.001	.443	.040
	HCHO	10.196	2715	<.001	8.499	.834
	AOD	29.828	2715	<.001	.045	.002
	$NO_2$	43.424	2715	.000	26.223	.604
	$O_3$	4.723	2715	<.001	.007	.002
	$SO_2$	-6.936	2715	<.001	-7.614	1.098

a simultaneous rise in both. However, the  $UHI_{index}$  shows a weaker correlation with other pollutants in urban areas, including aerosols,  $O_3$ , and  $SO_2$ . A notable observation is an inverse relationship between the  $UHI_{index}$  and  $SO_2$  in urban areas during the summer season. This suggests that as  $UHI$  effects become more intense,  $SO_2$  levels tend to decrease in urban areas during the summer.

#### 4.5. UPI indicator

Individual pollutant spatiotemporal maps struggle to effectively

reflect pollution levels over many areas. Nonetheless, the distinct samples *t*-test validates pollutant distribution spatial discrepancies. Furthermore, these maps, which focus on individual contaminants, fail to provide a comprehensive assessment of the combined impact of multiple pollutants. The research revealed a substantial link between the  $UHI$  indicator and the pollutants  $O_3$ ,  $NO_2$ , aerosols, HCHO, and CO in both urban and rural settings. In these circumstances, the  $UHI$  indicator demonstrates a substantial inverse connection with the pollutant  $SO_2$ . This highlights the necessity for a detailed observation of the link between  $UHI$  and contaminant. A  $UPI_{index}$  was created to evaluate the

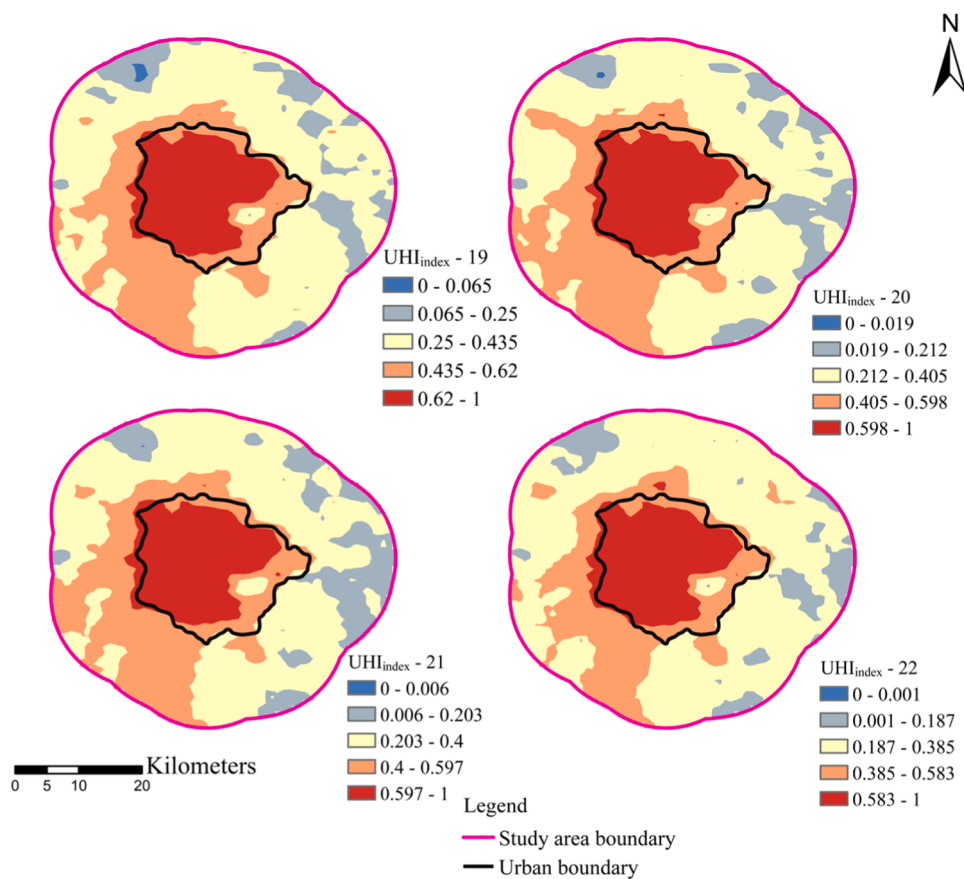


Fig. 5. Spatial distribution of UHI<sub>index</sub> in Bangalore 2019 - 2022.

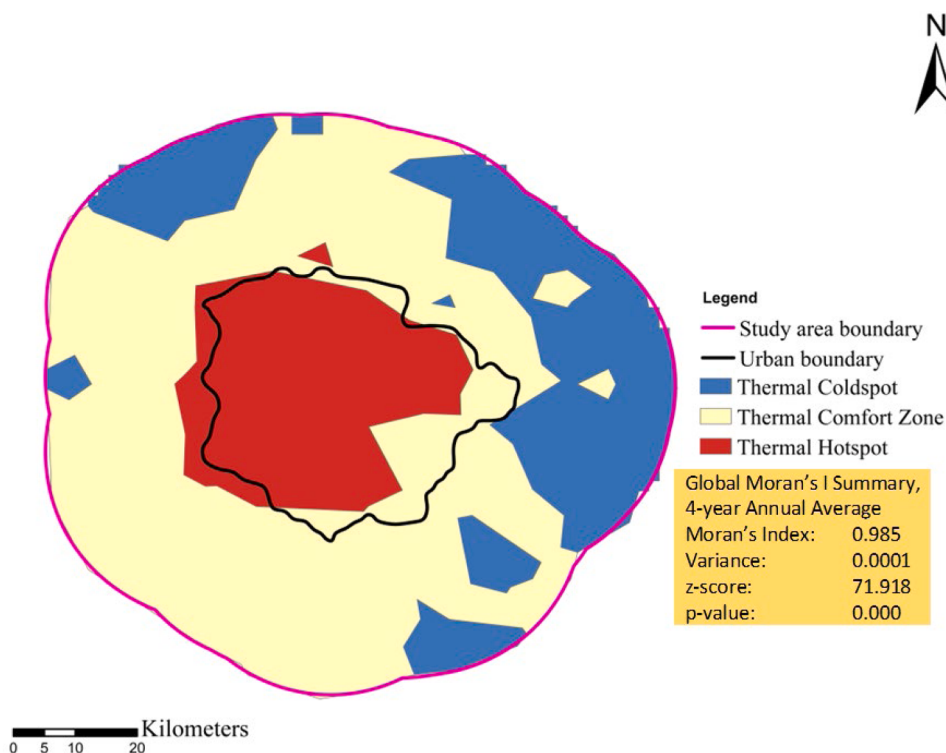
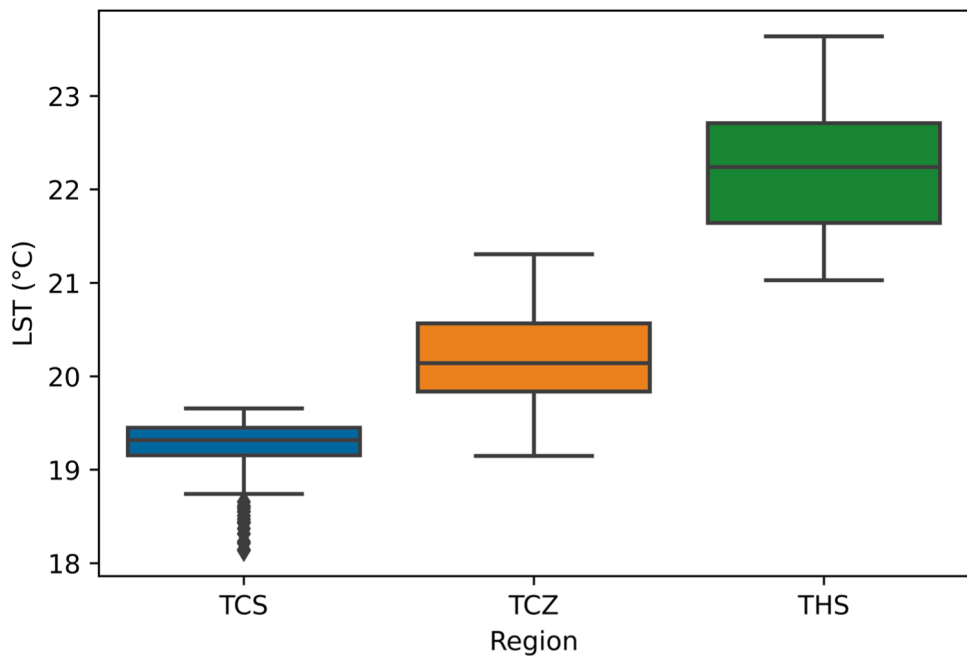


Fig. 6. Thermal classification of Bangalore.



**Fig. 7.** Comparison of four year mean yearly temperature in TCS, TCZ and THS.

**Table 3**

Correlation of various air contaminant with the  $UHI_{index}$ .

Region/Season	CO	HCHO	AOD	NO <sub>2</sub>	O <sub>3</sub>	SO <sub>2</sub>
Urban Annual	0.702	0.722	0.236	0.784	0.118	-0.05
Rural Annual	0.610	0.608	0.459	0.757	0.312	-0.157
Urban Summer	0.668	0.669	0.092	0.745	0.387	-0.176
Rural Summer	0.527	0.580	0.325	0.701	0.500	-0.062
Urban Winter	0.741	0.713	0.298	0.772	0.356	-0.057
Rural Winter	0.652	0.682	0.504	0.812	0.284	-0.237
Significance level: $p < 0.05$						
No correlation						
Positive correlation						
Negative correlation						

cumulative impacts of SO<sub>2</sub>, O<sub>3</sub>, HCHO, NO<sub>2</sub>, aerosols, and CO in specific locations and time periods. The weights of each pollutant are determined using the AHP and Fuzzy-AHP methods. The  $UPI_{index}$  is derived by using Eq. (7), as outlined in the data and methods section.

#### 4.5.1. Computation of weights for individual pollutants using AHP and fuzzy-AHP

Saaty [61] developed AHP, which is frequently utilized to solve complex decision-making challenges in the field of environmental and natural resource management. The AHP approach employs a  $6 \times 6$  matrix with diagonal entries set to one. This matrix is used to evaluate

**Table 4**

Saaty's scale of relative importance.

Intensity	9	7	5	3	1	2,4,6,8
Definition	Extreme importance	Very strong	Strong	Moderate	Equal importance	Intermediate values

component weights and facilitate comparisons. Analysis of expert perspectives and *t*-test findings is utilized to make comparative evaluations depend on Saaty's 1 to 9 scale (Table 4) to establish the relative relevance of essential features. The parameter weights are calculated by standardizing the pairwise comparisons (Table 5). To maintain the uniformity of the decision-making process, the Consistency Ratio (CR) is generated from the principal eigenvalue, which evaluates the coherence of the decision-making process.

Based on Brunelli (2014), the primary eigenvalue is an important indicator of matrix consistency. The maximum principal eigenvalue may be calculated by adding the eigenvectors from the pairwise matrix in Table 5 to the main eigenvalue matrix. In the instance of a 6 × 6 matrix, the major eigenvalue is 6.234. The computed numbers are then used to determine the Consistency Index (CI). The weights are normalized against Table 5. The primary eigenvalue is critical in determining the consistency of an idea via the CR, which is obtained using Eq. (12), whereas the CI is derived using Eq. (11) [61].

$$CI = (\lambda_{\max} - n) / (n - 1) \quad (11)$$

Where,

$n$  = number of parameters, and

$\lambda_{\max}$  = primary eigenvalue

Here,

$$CI = (6.234 - 6) / (6 - 1) = 0.047$$

$$CR = (CI / RI) \quad (12)$$

Where RI is the Random Index shown in Table 6

CI and CR are important measures in the AHP to ensure the consistency of the pairwise comparisons. The CI quantifies the deviation from perfect consistency, while the CR compares the CI to RI. A CR value below 10% (0.10) is crucial because it indicates that the judgments made in the pairwise comparison matrix are reasonably consistent. If the CR surpasses 10%, it implies inconsistencies in the comparisons, necessitating a revisit of the matrix to enhance accuracy. In this study, the calculated CR is 3.8%, which is well within the acceptable threshold, demonstrating the reliability of the judgments used to compute the pollutant weights.

The study suggests that the highest weight is NO<sub>2</sub> with 0.414, the remaining contaminant in urban settings, followed by AOD with a weight of 0.258, HCHO with a weight of 0.125, CO with a weight of 0.088, O<sub>3</sub> with a weight of 0.061, and SO<sub>2</sub> with a weight of 0.054. These parameters are essential for evaluating the combined effect of different contaminants on overall air quality. According to Lin et al. [64], the combination of Fuzzy logic and Fuzzy-AHP provides improved accuracy in multi-criteria evaluations. Fuzzy-AHP adeptly tackles the uncertainties and vagueness that naturally arise in intricate decision-making circumstances. It's an addition to the regular AHP that was made to deal with these issues by giving a structured way to judge and rank the importance of different factors in complicated decision-making processes.

The first stage in Fuzzy-AHP is to assign relative relevance to

**Table 5**  
AHP matrix and weights for pollutants.

Matrix	NO <sub>2</sub>	AOD	HCHO	CO	O <sub>3</sub>	SO <sub>2</sub>	Normalized principal Eigenvector
NO <sub>2</sub>	1	3	3	5	5	5	41.36%
AOD	1/3	1	3	3	5	5	25.82%
HCHO	1/3	1/3	1	1	3	3	12.53%
CO	1/5	1/3	1	1	1	2	8.83%
O <sub>3</sub>	1/5	1/5	1/3	1	1	1	6.08%
SO <sub>2</sub>	1/5	1/5	1/3	1/2	1	1	5.37%
Sum	2.27	5.07	8.67	11.50	16.00	17.00	
Total							100.00%

**Table 6**  
RI for various n scores.

n	RI
3	0.58
4	0.89
5	1.12
6	1.24
7	1.32
8	1.41
9	1.45
10	1.49

$$CR = (0.047 / 1.24) = 0.038 = 3.8\%.$$

individual contaminants in order to calculate weights. In contrast to conventional AHP, where the value "1" denotes equal priority, Fuzzy-AHP expresses equal importance as (1, 1, 1), encompassing the upper, middle, and lower values. Table 7 illustrates the assignment of Fuzzy numbers to the values 1, 2, 3, 5, 6, 7, 8, and 9 via a pairwise comparison matrix.

Reciprocal values, such as 1/2, 1/3, 1/5, and 1/6, are not directly translated to fuzzy numbers. Instead, Eq. (13) is used to calculate the inverse of fuzzy numbers.

$$A^{-1} = (l, m, u)^{-1} = (1 / u, 1 / m, 1 / l) \quad (13)$$

Where  $l$  =lower,  $m$  =middle, and  $u$  =upper.

The reciprocal value of 1/3 is seen in Table 5, namely in row 3 and column 2. Eq. (13) is used to calculate the equivalent fuzzy number, which is shown below:

$$A^{-1} = (2, 3, 4)^{-1} = (1 / 4, 1 / 3, 1 / 2).$$

Table 5 has been converted into a fuzzy form, as seen in Table 8. Buckley's (1985) geometric mean approach was utilised to calculate the fuzzy weights for every criterion, as well as the fuzzy geometric mean, as shown in Eq. (14).

$$\begin{aligned} \text{Fuzzygeometricmean} &= ((l_1, m_1, u_1) \times (l_2, m_2, u_2) \times \dots \times (l_n, m_n, u_n))^{1/n} \\ &= (l_1 \times l_2 \times \dots \times l_n)^{1/n}, (m_1 \times m_2 \times \dots \times m_n)^{1/n}, (u_1 \times u_2 \times \dots \times u_n)^{1/n} \end{aligned} \quad (14)$$

For example, Fuzzy geometric mean for NO<sub>2</sub>  
 $= (1 \times 2 \times 2 \times 4 \times 4 \times 4)^{1/6}, (1 \times 3 \times 3 \times 5 \times 5 \times 5)^{1/6}, (1 \times 4 \times 4 \times 6 \times 6 \times 6)^{1/6}$   
 $= (2.520, 3.225, 3.888)$

The  $r_i$  values are determined via the Fuzzy geometric mean.  $r_i = (2.520 + 1.587 + 0.794 + 0.589 + 0.437 + 0.364 + 3.225 + 2.054 + 1 + 0.715 + 0.487 + 0.434 + 3.888 + 2.57 + 1.26 + 0.849 + 0.561 + 0.561) / 14 = (6.290, 7.914, 9.690)$

Table 9 displays the fuzzy geometric mean, fuzzy weights, defuzzified weights, and weights adjusted to a standard or reference value for pollutants.

#### 4.5.2. UPI<sub>index</sub>

Fig. 8 depicts the yearly weighted mean UPI<sub>index</sub> over a four-year period, revealing higher levels of pollution in central urban regions, peri-urban areas, and the western section of the study area. While pollutant concentrations in rural areas are typically low to moderate, certain places within these regions have higher UPI<sub>index</sub> readings.

#### 4.6. Pollution risk map

The map of pollution risk divides the research region into distinct zones depending on pollutant concentrations. These zones include the LCZ, where pollutant levels are the lowest; the MCZ, where pollutant levels are moderate; and the HCZ, which has the peak pollutant levels. The Global Moran's I statistic z-scores for the contamination hazard map (Fig. 9) indicate less than a 1% chance that the observed clustering

**Table 7**

Fuzzified Saaty's scale.

Definition	Extreme importance	Very strong	Strong	Moderate	Equal importance	Intermediate values
Fuzzy-AHP Weights	(9,9,9)	(6,7,8)	(4,5,6)	(2,3,4)	(1,1,1)	(1,2,3), (3,4,5), (5,6,7), (7,8,9)
Intensity	9	7	5	3	1	2,4,6,8

**Table 8**

Fuzzified pairwise comparison matrix.

Matrix	NO <sub>2</sub>	AOD	HCHO	CO	O <sub>3</sub>	SO <sub>2</sub>	Fuzzy geometric mean value
NO <sub>2</sub>	(1,1,1)	(2,3,4)	(2,3,4)	(4,5,6)	(4,5,6)	(4,5,6)	(2.520, 3.225, 3.888)
AOD	(1/4,1/3,1/2)	(1,1,1)	(2,3,4)	(2,3,4)	(4,5,6)	(4,5,6)	(1.587, 2.054, 2.570)
HCHO	(1/4,1/3,1/2)	(1/4,1/3,1/2)	(1,1,1)	(1,1,1)	(2,3,4)	(2,3,4)	(0.794, 1.000, 1.260)
CO	(1/6,1/5,1/4)	(1/4,1/3,1/2)	(1,1,1)	(1,1,1)	(1,1,1)	(1,2,3)	(0.589, 0.715, 0.849)
O <sub>3</sub>	(1/6,1/5,1/4)	(1/6,1/5,1/4)	(1/4,1/3,1/2)	(1,1,1)	(1,1,1)	(1,1,1)	(0.437, 0.487, 0.561)
SO <sub>2</sub>	(1/6,1/5,1/4)	(1/6,1/5,1/4)	(1/4,1/3,1/2)	(1/3,1/2,1)	(1,1,1)	(1,1,1)	(0.364, 0.434, 0.561)
Total (r <sub>i</sub> )							(6.290, 7.914, 9.690)

**Table 9**

Fuzzy-AHP weights for the computation of UPI indicator.

Pollutant	Fuzzy geometric mean value	Calculation of Fuzzy weights = (l <sub>i</sub> , m <sub>i</sub> , u <sub>i</sub> ) x r <sub>i</sub> <sup>-1</sup>	Fuzzy weights	De-Fuzzified weights, d <sub>i</sub> = (Average of Fuzzy weights)	Normalized weights = d <sub>i</sub> /e
NO <sub>2</sub>	(2.520, 3.225, 3.888)	(2.520, 3.225, 3.888) x (1/9.690, 1/7.914, 1/6.290)	(0.260, 0.407, 0.618)	0.429	0.403
AOD	(1.587, 2.054, 2.570)	(1.587, 2.054, 2.570) x (1/9.690, 1/7.914, 1/6.290)	(0.164, 0.259, 0.409)	0.277	0.261
HCHO	(0.794, 1.000, 1.260)	(0.794, 1.000, 1.260) x (1/9.690, 1/7.914, 1/6.290)	(0.082, 0.126, 0.200)	0.136	0.128
CO	(0.589, 0.715, 0.849)	(0.589, 0.715, 0.849) x (1/9.690, 1/7.914, 1/6.290)	(0.061, 0.090, 0.135)	0.095	0.090
O <sub>3</sub>	(0.437, 0.487, 0.561)	(0.437, 0.487, 0.561) x (1/9.690, 1/7.914, 1/6.290)	(0.045, 0.062, 0.089)	0.065	0.061
SO <sub>2</sub>	(0.364, 0.434, 0.561)	(0.364, 0.434, 0.561) x (1/9.690, 1/7.914, 1/6.290)	(0.038, 0.055, 0.089)	0.061	0.057
Total			1.063	1.000	

pattern is due to random variation.

The contamination hazard map emphasizes the dependable occurrence of heightened levels of air pollutants in metropolitan areas, regardless of seasonal changes. The high contamination zones are primarily within urban areas, with some spillover into rural areas, particularly near urban boundaries. All seasons reveal higher pollutant concentrations in the heavily built-up Western region. Conversely, the

study area's rural areas host the majority of MCZs and LCZs.

The levels of pollution and LST have the minimal values in the LCZ, and the highest values in the HCZ. The box plots in Fig. 10 demonstrates a clear trend. The relationship between air pollutants and LST is crucial for understanding how urbanization affects both air quality and urban microclimates [70]. Increased LST, often resulting from the UHI effect, can lead to higher concentrations of certain air pollutants, such as O<sub>3</sub> and NO<sub>2</sub>, through accelerated chemical reactions in the atmosphere. Conversely, high levels of pollutants, especially aerosols and particulate matter, can influence LST by affecting the absorption and reflection of solar radiation. Understanding this interaction helps in identifying areas with poor air quality and high heat stress, which is essential for urban planning and developing strategies to mitigate the health impacts of UHI.

The ANOVA results, presented in Table 10, demonstrate a substantial disparity in the levels of LST and pollutants among the LCZ, MCZ, and HCZ. This disparity is statistically significant at a significance level of less than 0.001.

Table 11 presents a Post-Hoc analysis that thoroughly examines the differences in contaminant levels and LST among LCZ, MCZ, and HCZ during different seasons. It also includes the corresponding significant levels. The study shows a clear and consistent statistical trend: contaminant levels and LST are always higher in MCZ than in LCZ. On the other hand, pollutant levels and LST in HCZ are much higher than those in MCZ and LCZ, except for SO<sub>2</sub>. This pattern remains consistent throughout all seasons, with a level of significance lower than 0.001. While these differences are statistically significant, it is important to consider the practical implications of the findings. A statistically significant result does not necessarily imply that the observed differences are large enough to have a meaningful impact in real-world contexts. For example, although the difference in CO levels between HCZ and LCZ is statistically significant, its magnitude might not warrant immediate public health interventions or changes in urban planning policies. Furthermore, the results for O<sub>3</sub> during the winter season show an almost negligible mean difference between LCZ and HCZ (0.002) and are not statistically significant ( $p = 0.834$ ). This indicates that seasonal and pollutant-specific factors may influence the consistency of spatial patterns, as certain pollutants do not exhibit the expected trends across all conditions.

The comprehensive analysis, including Post-Hoc analyses, box plot analysis, and ANOVA, confirms that the pollution risk map of Bangalore effectively delineates and distinguishes areas with low and high quantities of contaminants across the research region. This advanced mapping tool is not only capable of accurately identifying regions with elevated pollutant levels but also serves as a foundation for developing targeted contaminant mitigation strategies, zoning rules, and customized initiatives for urban planning that address the particular needs and

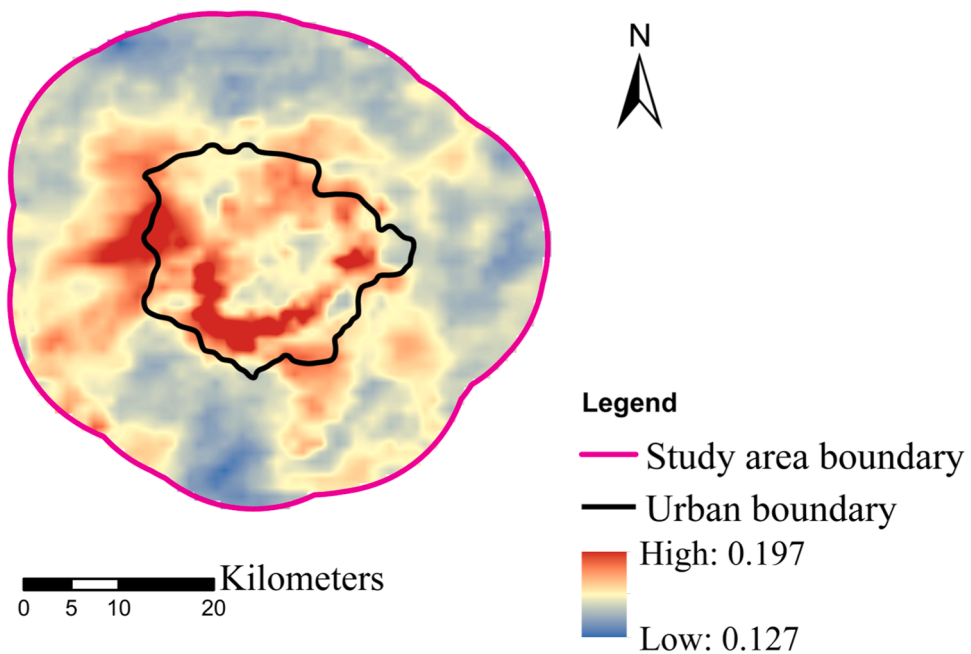
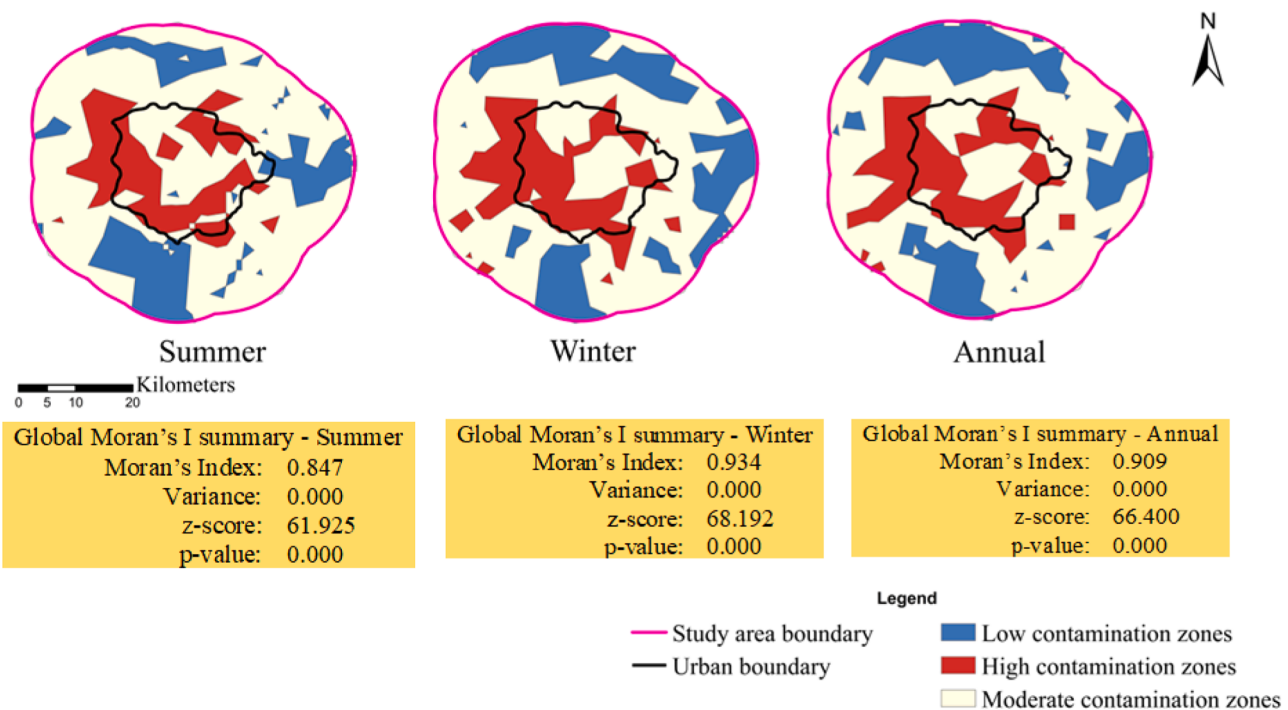
Fig. 8. Spatial distribution of  $UPI_{index}$  over Bangalore.

Fig. 9. Pollution risk map.

difficulties inherent to each specific area.

#### 4.7. Risk map

The High-Risk region refers to the area where the HCZ and THS zones intersect and where the residents experience elevated levels of air pollution and heat stress compared to the average. This research area, which has been divided into High-Risk Zones (HRZs) and Low Risk Zones (LRZs), is displayed in Fig. 11.

Table 12 provides a detailed analysis of the central tendency and dispersion of average yearly contaminant concentrations over a four-

year period in different pollution zones. HRZs have significantly higher yearly average concentrations of CO, HCHO, aerosols, and  $NO_2$  compared to LRZs, with increases of 2.028%, 8.816%, 13.610%, and 66.614%, respectively. The concentration of  $O_3$  in HRZs and LRZs is similar. On the other hand, LRZs have a higher yearly average concentration of  $SO_2$  compared to HRZs, exceeding it by 7.562%. The HRZs have an average LST that is 2.198 °C higher than LRZs. Several factors contribute to the observed differences in pollutant concentrations. Increased vehicular emissions, industrial activities, and higher population densities in urban areas largely drive the higher levels of  $NO_2$ , CO, and aerosols in HCZs. Socioeconomic factors such as rapid urbanization,

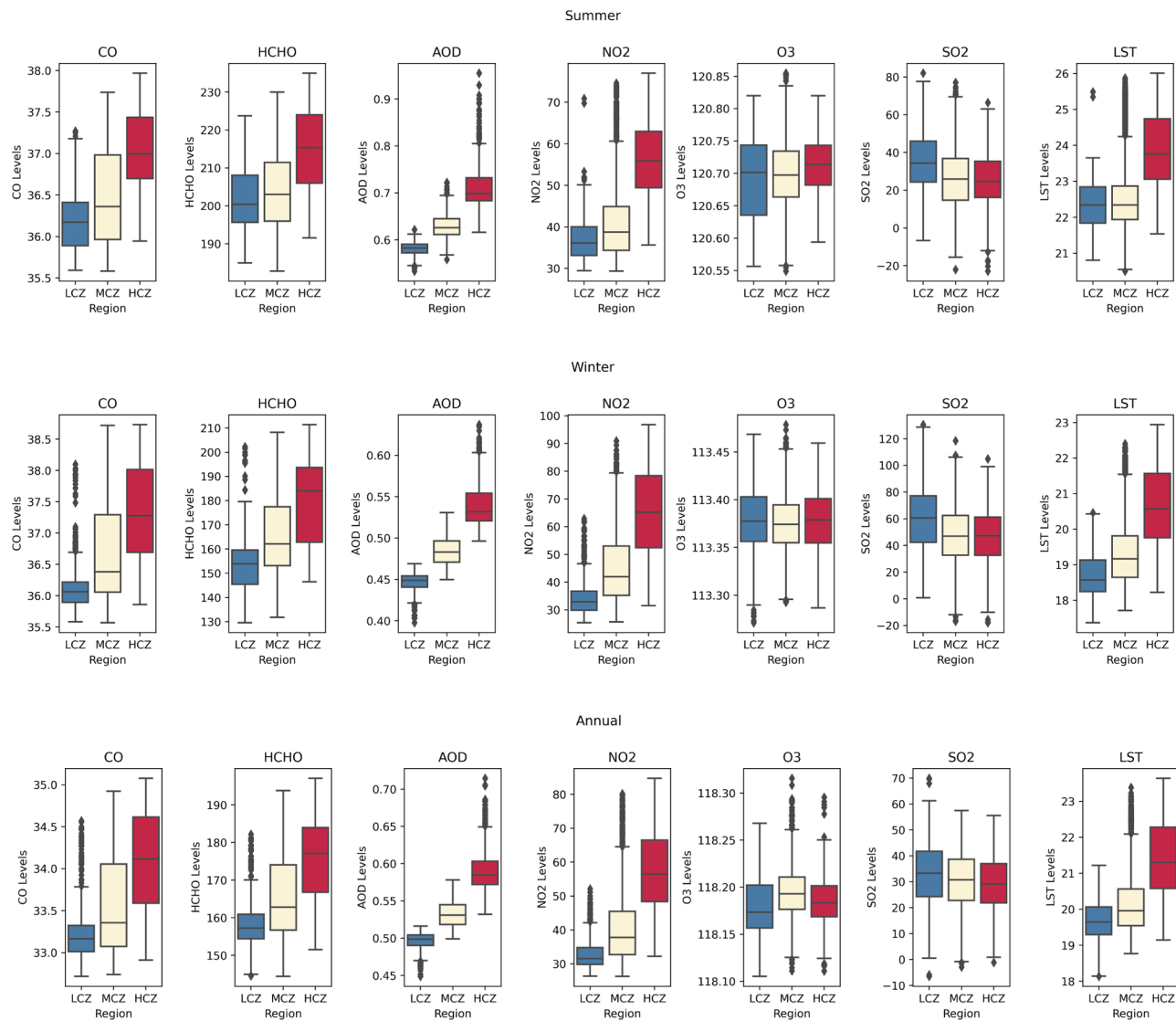


**Fig. 10.** The box plot distribution of the pollutants (CO (mmol/m<sup>2</sup>), HCHO (μmol/m<sup>2</sup>), AOD (unitless), NO<sub>2</sub> (μmol/m<sup>2</sup>), O<sub>3</sub> (mmol/m<sup>2</sup>), SO<sub>2</sub> (μmol/m<sup>2</sup>)) and LST (°C) in different pollutant regions.

**Table 10**  
ANOVA of pollutants and LST in various seasons.

Parameter	Season	Sum of Squares	Mean Square	F	Significance level
CO (mmol/m <sup>2</sup> )	Summer	171.820	85.910	321.924	<0.001
	Winter	432.946	216.473	375.736	<0.001
	Annual	202.669	101.334	331.969	<0.001
HCHO (μmol/m <sup>2</sup> )	Summer	53,239.453	26,619.727	275.183	<0.001
	Winter	195,770.046	97,885.023	403.270	<0.001
	Annual	88,454.087	44,227.043	447.407	<0.001
AOD (Unitless)	Summer	4.597	2.299	2843.017	.000
	Winter	2.684	1.342	4060.669	.000
	Annual	2.723	1.362	3726.674	.000
NO <sub>2</sub> (μmol/m <sup>2</sup> )	Summer	106,465.819	53,232.910	661.104	<0.001
	Winter	301,727.624	150,863.812	951.736	.000
	Annual	189,359.593	94,679.797	851.557	<0.001
O <sub>3</sub> (mmol/m <sup>2</sup> )	Summer	.161	.081	27.232	<0.001
	Winter	.003	.002	1.588	.204
	Annual	.104	.052	61.897	<0.001
SO <sub>2</sub> (μmol/m <sup>2</sup> )	Summer	35,321.174	17,660.587	70.629	<0.001
	Winter	79,376.659	39,688.330	78.443	<0.001
	Annual	5949.281	2974.641	23.134	<0.001
LST (°C)	Summer	755.670	377.835	430.939	<0.001
	Winter	1153.021	576.510	653.623	<0.001
	Annual	945.605	472.803	596.318	<0.001

**Table 11**

Post-Hoc analysis of LST and pollutants in various pollution zones.

Parameter	Season	(I) Zone	(J) Zone	Mean Difference (I-J)	Std. Error	Significance level
CO (mmol/m <sup>2</sup> )	Summer	LCZ	MCZ	-0.251	.022	<0.001
			HCZ	-0.800	.028	<0.001
	Winter	LCZ	MCZ	-0.593	.027	<0.001
			HCZ	-1.210	.038	.000
	Annual	LCZ	MCZ	-0.336	.021	.000
			HCZ	-0.837	.029	<0.001
HCHO (μmol/m <sup>2</sup> )	Summer	LCZ	MCZ	-2.090	.455	<0.001
			HCZ	-12.964	.622	<0.001
	Winter	LCZ	MCZ	-12.728	.605	.000
			HCZ	-25.724	.823	<0.001
	Annual	LCZ	MCZ	-6.595	.379	.000
			HCZ	-17.400	.520	<0.001
AOD (Unitless)	Summer	LCZ	MCZ	-0.049	.001	.000
			HCZ	-0.133	.002	.000
	Winter	LCZ	MCZ	-0.038	.001	.000
			HCZ	-0.095	.001	.000
	Annual	LCZ	MCZ	-0.036	.001	.000
			HCZ	-0.096	.001	.000
NO <sub>2</sub> (μmol/m <sup>2</sup> )	Summer	LCZ	MCZ	-4.258	.334	.000
			HCZ	-19.046	.492	.000
	Winter	LCZ	MCZ	-10.857	.426	<0.001
			HCZ	-31.608	.747	.000
	Annual	LCZ	MCZ	-8.024	.347	<0.001
			HCZ	-25.041	.567	.000
O <sub>3</sub> (mmol/m <sup>2</sup> )	Summer	LCZ	MCZ	-0.008	.003	.040
			HCZ	-0.025	.003	<0.001
	Winter	LCZ	MCZ	.003	.002	.264
			HCZ	.002	.002	.834
	Annual	LCZ	MCZ	-0.014	.001	<0.001
			HCZ	-0.004	.002	.045
SO <sub>2</sub> (μmol/m <sup>2</sup> )	Summer	LCZ	MCZ	8.921	.776	<0.001
			HCZ	10.029	.987	<0.001
	Winter	LCZ	MCZ	12.336	1.063	<0.001
			HCZ	13.365	1.320	<0.001
	Annual	LCZ	MCZ	3.067	.576	<0.001
			HCZ	4.287	.676	<0.001
LST ( °C)	Summer	LCZ	MCZ	-0.241	.036	.000
			HCZ	-1.540	.056	.000
	Winter	LCZ	MCZ	-0.636	.035	.000
			HCZ	-1.946	.054	.000
	Annual	LCZ	MCZ	-0.467	.034	.000
			HCZ	-1.735	.051	<0.001

industrial growth, and expanding infrastructure significantly contribute to elevated pollutant levels. For instance, dense transportation networks and greater energy consumption in urban regions play a critical role in the increased concentrations of these pollutants. In contrast, rural areas typically experience lower pollutant levels due to the absence of large-scale industrial activity and lower population density. However, pollutant spillover into rural areas can occur due to atmospheric transportation and regional weather patterns, especially when industrial zones are located near urban-rural boundaries. The HRZ encompasses the regions of Uttarahalli, Yeshwanthpura, K R Pura, and others, as illustrated in Fig. 11.

The division of regions into HRZ and LRZ according to pollutant concentrations reveals critical disparities essential for tailored interventions. HRZ demonstrates notably higher annual average concentrations of CO, HCHO, aerosols, and NO<sub>2</sub> compared to LRZ. Interestingly, ozone concentrations exhibit relative similarity between these zones. However, HRZ notably experiences elevated LST, emphasizing the pronounced influence of UHI on localized temperature variations.

## 5. Conclusions

The comprehensive study investigated the intricate relationship between various pollutants and UHI effects in Bangalore from 2019 to 2022 and sheds light on critical dynamics impacting climate dynamics, urban ecology, and the annual weighted average of the well-being of

urban dwellers. Higher levels of O<sub>3</sub>, NO<sub>2</sub>, aerosols, HCHO, and CO were found in urban areas compared to rural areas. This study shows how contaminant concentrations are very different between urban and rural areas. These results highlight the critical need for targeted actions to mitigate the adverse effects of urbanization on air quality.

The correlation analysis between UHI indicators and pollutants across urban-rural settings presents compelling evidence of their interdependence. Positive associations observed between UHI indicators and several pollutants NO<sub>2</sub>, O<sub>3</sub>, CO, HCHO, and aerosols highlight the amplified pollution levels in areas experiencing more pronounced UHI effects. Conversely, the negative correlation between UHI indicators and SO<sub>2</sub> could be due to the complex chemical and physical interactions between SO<sub>2</sub> and the atmospheric conditions within urban areas. One plausible explanation is that SO<sub>2</sub>, which can form sulfate aerosols, has a cooling effect by reflecting solar radiation, counteracting the warming effect of the UHI. Furthermore, the urban boundary layer can limit the vertical mixing of air, trapping pollutants such as CO and NO<sub>2</sub> while allowing SO<sub>2</sub> to disperse more quickly. Another possible factor is the increased industrial regulation in urban areas, leading to lower SO<sub>2</sub> emissions compared to rural areas, especially during hotter periods when UHI effects are more pronounced.

The stratification of areas into HRZs and LRZs based on pollutant concentrations unveils disparities crucial for targeted interventions. HRZs exhibit significantly higher yearly average concentrations of CO, HCHO, aerosols, and NO<sub>2</sub> compared to LRZs, i.e., an increase in CO, HCHO, and NO<sub>2</sub> concentrations in HRZs compared to LRZs, such as CO

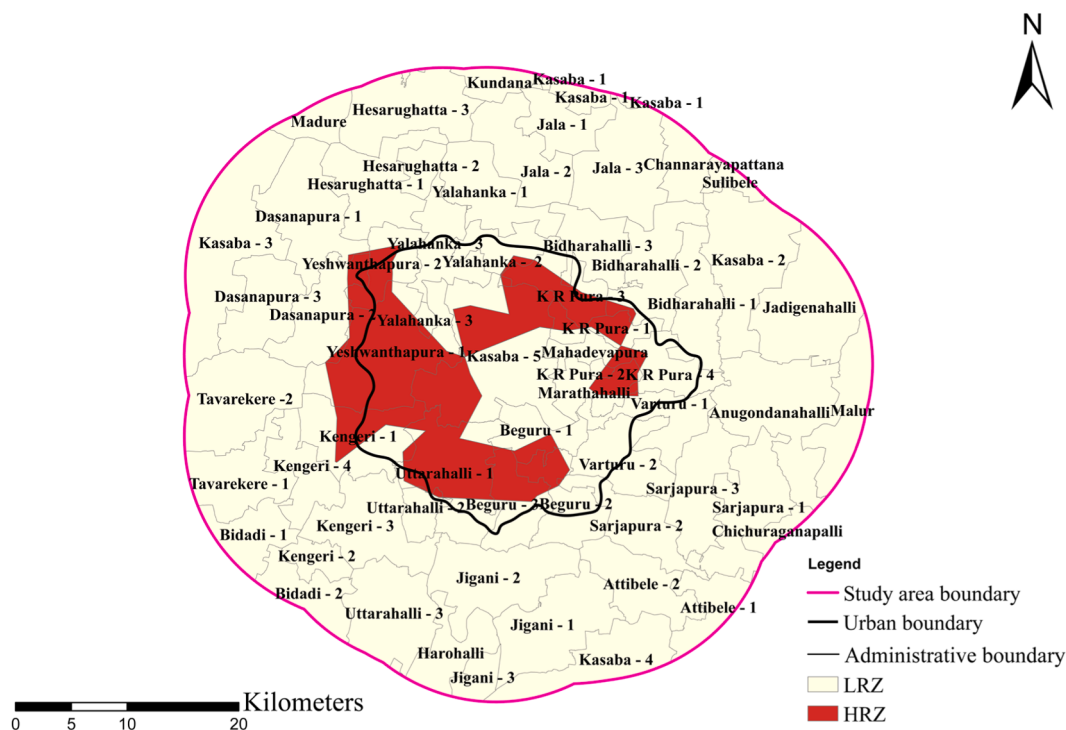


Fig. 11. Risk map.

**Table 12**  
LST and Pollutant concentrations.

Parameter	Zone	Mean	Standard Deviation
CO (mmol/m <sup>2</sup> )	LRZ	33.529	.590
	HRZ	34.209	.473
HCHO (μmol/m <sup>2</sup> )	LRZ	164.150	10.675
	HRZ	178.623	9.384
Aerosols (Unitless)	LRZ	.529	.029
	HRZ	.601	.036
NO <sub>2</sub> (μmol/m <sup>2</sup> )	LRZ	39.724	10.683
	HRZ	66.186	10.303
O <sub>3</sub> (mmol/m <sup>2</sup> )	LRZ	118.190	.030
	HRZ	118.184	.023
SO <sub>2</sub> (μmol/m <sup>2</sup> )	LRZ	30.735	11.488
	HRZ	28.574	10.779
LST ( °C)	LRZ	20.110	.834
	HRZ	22.308	.702

concentrations being 2.028% higher, HCHO concentrations increasing by 8.816%, and NO<sub>2</sub> levels being 66.614% higher in HRZs. Notably, while ozone concentrations remain relatively similar between the zones, HRZs show LSTs 2.198 °C higher than in LRZs, accentuating the impact of UHI on local temperature variations.

These findings hold substantial implications for urban planning and policy formulation, i.e., urban heat mitigation policies, stricter emission controls, sustainable urban development, and climate-resilient infrastructure. The insights gleaned from this research provide a foundation for informed decision-making in implementing tailored techniques designed to reduce the negative effects of UHI and pollution, i.e., UHI effects can elevate local temperatures, which in turn influences air pollutant concentrations. Higher temperatures increase the rate of photochemical reactions, leading to elevated concentrations of pollutants such as O<sub>3</sub>. Additionally, UHI can trap pollutants in the lower atmosphere due to temperature inversions, especially at night, resulting in higher levels of CO, NO<sub>2</sub>, and aerosols. However, it is important to acknowledge the limitations of this study. Firstly, the data collection methods primarily relied on satellite data and remote sensing

techniques, which, while useful, may have certain limitations in resolution and accuracy, particularly in smaller geographic areas. Secondly, the scope of the study focused on Bangalore, and as such, the findings may not be directly applicable to other regions with different climatic, socio-economic, or geographic characteristics. Lastly, the AHP method's use of expert judgment may introduce potential biases, despite efforts to maintain consistency in the decision-making processes. Furthermore, the reduction in vegetation and open spaces within urban areas exacerbates the effect, as vegetation typically helps mitigate air pollution by absorbing pollutants and providing cooling through evapotranspiration. These combined effects of UHI amplify pollutant levels, leading to poor air quality in urban areas. Solutions might encompass green infrastructure implementation, the creation of urban green spaces, stringent emission controls, and targeted zoning regulations to curtail pollution hotspots.

## Funding

This work received financial support from the Science and Engineering Research Board (SERB), a statutory body of the Department of Science & Technology (DST), Government of India, with grant number SRG/2021/002,067.

## CRediT authorship contribution statement

**Aneesh Mathew:** Writing – review & editing, Visualization, Supervision, Methodology, Investigation, Conceptualization. **K.S. Arunab:** Writing – original draft, Validation, Software, Resources, Methodology, Data curation, Conceptualization.

## Declaration of competing interest

The authors declare that they have no known competing financial interests or personal relationships that could have appeared to influence the work reported in this paper.

## Acknowledgments

This work was supported by the Science and Engineering Research Board (SERB), a statutory body of the Department of Science and Technology (DST), under grant number SRG/2021/002067. The authors also wish to thank the U.S. Geological Survey (USGS) and European Space Agency (ESA) for making available the satellite data. The authors wish to thank anonymous reviewers for their constructive comments to improve the quality of the manuscript.

## Data availability statement

The datasets generated and/or analyzed during the current study are available upon reasonable request from the corresponding author.

## Supplementary materials

Supplementary material associated with this article can be found, in the online version, at [doi:10.1016/j.solcom.2025.100108](https://doi.org/10.1016/j.solcom.2025.100108).

## References

- [1] R. Anniballe, S. Bonafoni, M. Pichiari, Spatial and temporal trends of the surface and air heat island over Milan using MODIS data, *Remote Sens. Environ.* 150 (2014) 163–171.
- [2] A.M. Rizwan, L.Y. Dennis, L.I.U. Chunho, A review on the generation, determination and mitigation of Urban Heat Island, *J. Environ. Sci.* 20 (1) (2008) 120–128.
- [3] S. Arshad, S.R. Ahmad, S. Abbas, A. Asharf, N.A. Siddiqui, Z. ul Islam, Quantifying the contribution of diminishing green spaces and urban sprawl to urban heat island effect in a rapidly urbanizing metropolitan city of Pakistan, *Land Use Pol.* 113 (2022) 105874.
- [4] V. Ferrara, A. Ekbom, A. Wästfelt, Biocultural heritage in Sicilian olive groves: the importance of heterogeneous landscapes over the long term, *Encyclop. World's Biomes.* (2020) 135–145.
- [5] UN EPA, 2022. <https://population.un.org/wpp/>.
- [6] Y. Gao, J. Zhao, L. Han, Exploring the spatial heterogeneity of urban heat island effect and its relationship to block morphology with the geographically weighted regression model, *Sustain. Cities Society* 76 (2022) 103431.
- [7] S.W. Kim, R.D. Brown, UHI intensity and magnitude estimations: a systematic literature review, *Sci. Total Environ.* 779 (2021) 146389.
- [8] T.R. Oke, The energetic basis of the urban heat island, *Quarterly journal of the royal meteorological society* 108 (455) (1982) 1–24.
- [9] K.S. Arunab, A. Mathew, Geospatial and statistical analysis of urban heat islands and thermally vulnerable zones in Bangalore and Hyderabad cities in India, *Remote Sens. Appl.* 32 (2023) 101049.
- [10] M.A.A. Gazi, I. Mondal, Urban heat island and its effect on dweller of Kolkata metropolitan area using geospatial techniques, *Int. J. Comp. Sci. Eng.* 6 (10) (2018) 741–753.
- [11] J.M. Hassell, M. Begon, M.J. Ward, E.M. Fèvre, Urbanization and disease emergence: dynamics at the wildlife–livestock–human interface, *Trend. Ecol. Evolut.* 32 (1) (2017) 55–67.
- [12] A.M. Thompson, B.G. Doddrige, J.C. Witte, R.D. Hudson, W.T. Luke, J.E. Johnson, R. Weller, A tropical Atlantic paradox: shipboard and satellite views of a tropospheric ozone maximum and wave-one in January–February 1999, *Geophys. Res. Lett.* 27 (20) (2000) 3317–3320.
- [13] H. Li, F. Meier, X. Lee, T. Chakraborty, J. Liu, M. Schaap, S. Sodoudi, Interaction between urban heat island and urban pollution island during summer in Berlin, *Sci. Total Environ.* 636 (2018) 818–828.
- [14] K.S. Arunab, A. Mathew, Quantifying urban heat island and pollutant nexus: a novel geospatial approach, *Sustain. Cities Society* 101 (2024) 105117.
- [15] G. Guerri, A. Crisci, A. Messeri, L. Congedo, M. Munafò, M. Morabito, Thermal summer diurnal hot-spot analysis: the role of local urban features layers, *Remote Sens.* 13 (3) (2021) 538.
- [16] A. Mathew, S. Khandelwal, N. Kaul, Spatial and temporal variations of urban heat island effect and the effect of percentage impervious surface area and elevation on land surface temperature: study of Chandigarh city, India, *Sustain. Cities Society* 26 (2016) 264–277.
- [17] H. Radhi, E. Assem, S. Sharples, On the colours and properties of building surface materials to mitigate urban heat islands in highly productive solar regions, *Build. Environ.* 72 (2014) 162–172.
- [18] Hibbard, K., Hoffman, F.M., Huntzinger, D., & West, T. O. (2017). Ch. 10: changes in land cover and terrestrial biogeochemistry. Climate science Special Report: fourth National Climate Assessment, Volume I (DJ Wuebbles, DW Fahey, KA Hibbard, DJ Dokken, BC Stewart, & TK Maycock.
- [19] A.K. Pandey, S. Singh, S. Berwal, D. Kumar, P. Pandey, A. Prakash, K. Kumar, Spatio-temporal variations of urban heat island over Delhi, *Urban Clim.* 10 (2014) 119–133.
- [20] K. Kourtidis, A.K. Georgoulias, S. Rapsomanikis, V. Amiridis, I. Keramitsoglou, H. Hooyberghs, D. Melas, A study of the hourly variability of the urban heat island effect in the Greater Athens Area during summer, *Sci. Total Environ.* 517 (2015) 162–177.
- [21] A. Mathew, S. Khandelwal, N. Kaul, Investigating spatial and seasonal variations of urban heat island effect over Jaipur city and its relationship with vegetation, urbanization and elevation parameters, *Sustain. Citie. Society* 35 (2017) 157–177.
- [22] G. Grigoraş, B. Urătescu, Spatial hotspot analysis of Bucharest's UHI using modis data, *Annal. Valahia Univer. Targoviste. Geograph. Series* 18 (1) (2018) 14–22.
- [23] S. Shahfahad, Talukdar, M. Rihan, H.T. Hang, S. Bhaskaran, A. Rahman, Modelling UHI and thermal field variation and their relationship with land use indices over Delhi and Mumbai metro cities, *Environ., Develop. Sustain.* (2021) 1–29.
- [24] J.H. Seinfeld, S.N. Pandis, *Atmospheric Chemistry and physics: from Air Pollution to Climate Change*, John Wiley & Sons, 2016.
- [25] T.M. Giannaros, D. Melas, I.A. Daglis, I. Keramitsoglou, K. Kourtidis, Numerical study of the urban heat island over Athens (Greece) with the WRF model, *Atmosph. Environ.* 73 (2013) 103–111.
- [26] M. Santamouris, S. Haddad, M. Saliari, K. Vasilakopoulou, A. Synnefa, R. Paolini, F. Fiorito, On the energy impact of urban heat island in Sydney: climate and energy potential of mitigation technologies, *Energy Build.* 166 (2018) 154–164.
- [27] B.N. Holben, T.F. Eck, I.A. Slutsker, D. Tanré, J.P. Buis, A. Setzer, A. Smirnov, AERONET—A federated instrument network and data archive for aerosol characterization, *Remote Sens. Environ.*, 66 (1) (1998) 1–16.
- [28] Z. Haizhu, Z. Neng, W. Qingqin, Modelling and simulation of the urban heat island effect in a tropical seaside city considering multiple street canyons, *Indoor Built Environ.* 30 (8) (2021) 1124–1141.
- [29] M.T. Simmons, B. Gardiner, S. Windhager, J. Tinsley, Green roofs are not created equal: the hydrologic and thermal performance of six different extensive green roofs and reflective and non-reflective roofs in a sub-tropical climate, *Urban Ecosyst.* 11 (2008) 339–348.
- [30] B. Halder, J. Bandyopadhyay, P. Banik, Monitoring the effect of urban development on urban heat island based on remote sensing and geo-spatial approach in Kolkata and adjacent areas, India, *Sustain. Cities Society* 74 (2021) 103186.
- [31] G. Ulpiani, On the linkage between urban heat island and urban pollution island: three-decade literature review towards a conceptual framework, *Sci. Total Environ.* 751 (2021) 141727.
- [32] Z. Qiao, G. Tian, L. Xiao, Diurnal and seasonal impacts of urbanization on the urban thermal environment: a case study of Beijing using MODIS data, *ISPRS J. Photogramm. Remote Sens.* 85 (2013) 93–101.
- [33] A. Mathew, S. Khandelwal, N. Kaul, S. Chauhan, Analyzing the diurnal variations of land surface temperatures for surface urban heat island studies: Is time of observation of remote sensing data important? *Sustainable cities and society* 40 (2018) 194–213.
- [34] Y. Wang, Z. Guo, J. Han, The relationship between urban heat island and air pollutants and them with influencing factors in the Yangtze River Delta, China, *Ecol. Indicators* 129 (2021) 107976.
- [35] A. Bhargava, S. Lakmini, S. Bhargava, *Urban Heat Island Effect: its relevance in urban planning*, *J. Biodivers. Endanger. Species* 5 (187) (2017) 2020.
- [36] Lake 2010: Wetlands, biodiversity and climate change.
- [37] R. Kesavan, M. Muthian, K. Sudalaimuthu, S. Sundarsingh, S. Krishnan, ARIMA modeling for forecasting land surface temperature and determination of urban heat island using remote sensing techniques for Chennai city, India, *Arab. J. Geosci.* 14 (11) (2021) 1016.
- [38] S. Guha, H. Govil, S. Mukherjee, Dynamic analysis and ecological evaluation of urban heat islands in Raipur city, India, *J. Appl. Remote Sens.* 11 (3) (2017), 036020–036020.
- [39] World Population Review. (2024). Bangalore, India population 2024. Retrieved from <https://worldpopulationreview.com/world-cities/bangalore-population>.
- [40] T.V. Ramachandra, K.S. Asulabha, V. Sincy, A. Baghel, S. Vinay, Bangalore Lakes Information System (BLIS) for Sustainable Management of Lakes, *J. Indian Inst. Sci.* (2024) 1–20.
- [41] S. Cheval, A. Dumitrescu, The July urban heat island of Bucharest as derived from MODIS images, *Theor. Appl. Climatol.*, 96 (2009) 145–153.
- [42] O. Rozenstein, Z. Qin, Y. Derimian, A. Karnieli, Derivation of land surface temperature for Landsat-8 TIRS using a split window algorithm, *Sensors* 14 (4) (2014) 5768–5780.
- [43] C.R. Nowlan, G. González Abad, H.A. Kwon, Z. Ayazpour, C. Chan Miller, K. Chance, K. Sun, Global formaldehyde products from the ozone mapping and profiler suite (OMPS) nadir mappers on Suomi NPP and NOAA-20, *Earth Space Sci.* 10 (5) (2023) e2022EA002643.
- [44] H.C. Huang, S. Zheng, Z. Zhao, Application of Pearson correlation coefficient (PCC) and Kolmogorov-Smirnov distance (KSD) metrics to identify disease-specific biomarker genes, *Bmc Bioinform.* 11 (2010) 1–2.
- [45] M.K. Mishra, A. Mathew, Investigating the spatio-temporal correlation between urban heat island and atmospheric pollution island interaction over Delhi, India using geospatial techniques, *Arab. J. Geosci.* 15 (20) (2022) 1591.
- [46] G. Suthar, R.P. Singhal, S. Khandelwal, N. Kaul, Spatiotemporal variation of air pollutants and their relationship with land surface temperature in Bengaluru, India, *Remote Sens. Appl.* 32 (2023) 101011.
- [47] D.X. Tran, F. Pla, P. Latorre-Carmona, S.W. Myint, M. Caetano, H.V. Kieu, Characterizing the relationship between land use land cover change and land surface temperature, *ISPRS J. Photogramm. Remote Sens.* 124 (2017) 119–132.
- [48] Y. Zhang, I.O. Odeh, C. Han, Bi-temporal characterization of land surface temperature in relation to impervious surface area, NDVI and NDBI, using a sub-pixel image analysis, *Int. J. Appl. Earth Observ. Geoinform.* 11 (4) (2009) 256–264.

- [49] B.C. Gao, NDWI—A normalized difference water index for remote sensing of vegetation liquid water from space, *Remote Sens. Environ.* 58 (3) (1996) 257–266.
- [50] C.T. Nguyen, A. Chidthaisong, P. Kieu Diem, L.Z. Huo, A modified bare soil index to identify bare land features during agricultural fallow-period in southeast Asia using Landsat 8, *Land* 10 (3) (2021) 231.
- [51] Szabo, S., Gács, Z., & Balazs, B. (2016). Specific features of NDVI, NDWI and MNDWI as reflected in land cover categories.
- [52] Y. Zha, J. Gao, S. Ni, Use of normalized difference built-up index in automatically mapping urban areas from TM imagery, *Int. J. Remote Sens.* 24 (3) (2003) 583–594.
- [53] B. Kavhu, K.S. Mpakairi, Spatial Monitoring and Reporting Tool (SMART) in Mid-Zambezi Valley, Zimbabwe: Implementation challenges and practices, *Conservation Science and Practice* 3 (9) (2021) e492.
- [54] Setturu, B., Kumar, U., & Ramachandra, T.V. Spatio-temporal pattern of landuse dynamics for Bangalore.
- [55] Haynes, K.B. (2020). The urban morphology of Hyderabad, India: a historical geographic analysis.
- [56] M. Valipour, Optimization of neural networks for precipitation analysis in a humid region to detect drought and wet year alarms, *Meteorol. Applic.* 23 (1) (2016) 91–100.
- [57] A. Siddiqui, G. Kushwaha, B. Nikam, S.K. Srivastav, A. Shelar, P. Kumar, Analysing the day/night seasonal and annual changes and trends in land surface temperature and surface urban heat island intensity (SUHII) for Indian cities, *Sustain. Citie. Society* 75 (2021) 103374.
- [58] A. Badugu, K.S. Arunab, A. Mathew, P. Sarwesh, Spatial and temporal analysis of urban heat island effect over Tiruchirappalli city using geospatial techniques, *Geodesy Geodynam.* 14 (3) (2023) 275–291.
- [59] R. Bala, R. Prasad, V.P. Yadav, Quantification of urban heat intensity with land use/land cover changes using Landsat satellite data over urban landscapes, *Theor. Appl. Climatol.* 145 (2021) 1–12.
- [60] U. Rajasekar, Q. Weng, Urban heat island monitoring and analysis using a non-parametric model: a case study of Indianapolis, *ISPRS Journal of Photogramm. Remote Sens.* 64 (1) (2009) 86–96.
- [61] T.L. Saaty, The analytic hierarchy process (AHP), *J. Operat. Res. Society* 41 (11) (1980) 1073–1076.
- [62] P.R. Shekar, A. Mathew, Delineation of groundwater potential zones and identification of artificial recharge sites in the Kinnerasani Watershed, India, using remote sensing-GIS, AHP, and fuzzy-AHP techniques, *AQUA—Water Infrastructure, Ecosystems and Society* 72 (8) (2023) 1474–1498.
- [63] H.M. Lyu, W.J. Sun, S.L. Shen, A. Arulrajah, Flood risk assessment in metro systems of mega-cities using a GIS-based modeling approach, *Sci. Total Environ.* 626 (2018) 1012–1025.
- [64] Y. Lin, X. Li, Y. Hu, Deep diagnostics and prognostics: an integrated hierarchical learning framework in PHM applications, *Appl. Soft Comp.* 72 (2018) 555–564.
- [65] P.A. Moran, Notes on continuous stochastic phenomena, *Biometrika* 37 (1/2) (1950) 17–23.
- [66] M.D.K.L. Gunathilaka, W.T.S. Harshana, Evaluation of urban heat island (UHI) spatial change in freshwater lakes with hot spot analysis (GI statistics), *Int. J. Environ., Eng. Educ.* 3 (2) (2021) 48–58.
- [67] J.K. Ord, A. Getis, Local spatial autocorrelation statistics: distributional issues and an application, *Geograph. Anal.* 27 (4) (1995) 286–306.
- [68] A. Mitchell, The ESRI Guide to GIS Analysis, Environmental Systems Research Institute, 1999 (Vol. 3).
- [69] G. Suthar, R.P. Singhal, S. Khandelwal, N. Kaul, Spatiotemporal variation of air pollutants and their relationship with land surface temperature in Bengaluru, India, *Remote Sens. Applic.* 32 (2023) 101011.
- [70] S.L. Harlan, D.M. Ruddell, Climate change and health in cities: impacts of heat and air pollution and potential co-benefits from mitigation and adaptation, *Curr. Opinion Environ. Sustain.* 3 (3) (2011) 126–134.